STUDY OF CALCIUM OXIDE-MANGANESE OXIDE ADSORBENT ON CARBON DIOXIDE CAPTURE

LOW WEI FOO

A project report submitted in partial fulfilment of the requirements for the award of Bachelor of Engineering (Honours) Chemical Engineering

Lee Kong Chian Faculty of Engineering and Science
Universiti Tunku Abdul Rahman

April 2019

DECLARATION

I hereby declare that this project report is based on my original work except for citations and quotations which have been duly acknowledged. I also declare that it has not been previously and concurrently submitted for any other degree or award at UTAR or other institutions.

Signature : _____

Name : Low Wei Foo

ID No. : 14UEB01587

Date : _____

APPROVAL FOR SUBMISSION

I certify that this project report entitled **"STUDY OF CALCIUM OXIDE-MANGANESE OXIDE ADSORBENT ON CARBON DIOXIDE CAPTURE"** was prepared by **LOW WEI FOO** has met the required standard for submission in partial fulfilment of the requirements for the award of Bachelor of Engineering (Honours) Chemical Engineering at Universiti Tunku Abdul Rahman.

Approved by,

Signature : _____

Supervisor : Dr. Lee Zhi Hua

Date : _____

ACKNOWLEDGEMENTS

I would like to thank everyone who had contributed to the successful completion of this project. I would like to express my gratitude to my research supervisor, Dr. Lee Zhi Hua for her invaluable advice, guidance and her enormous patience throughout the development of the research.

In addition, I would also like to express my gratitude to my loving parents and friends who had helped and given me encouragement during my project time. I would like to specially thanks Ms. Vitiyaa a/p Selva Kumar for her guidance and helps on laboratory instruments procedures. Without all their guidance and knowledge, this research will not be completed.

ABSTRACT

Calcium oxide added with transition metal oxide and its potential towards adsorption of carbon dioxide were investigated in this project. Calcium oxide with the addition of manganese oxide were synthesized and its efficiency in absorbing carbon dioxide has been studied. Calcium oxide, CaO added with manganese oxide, MnO were synthesized by sol-gel method. The obtained powdered particles and pure CaO adsorbent were characterised using SEM and EDX techniques. XRD analysis is performed on the CaO and CaO-MnO adsorbent to determine the components present and calculate the mean crystallite size. The CO_2 adsorption rate and capacity of the CaO-MnO adsorbent is determined by passing carbon dioxide gas through it using Thermogravimetric Analyser (TGA) at carbonation temperature of 463, 500 and 590 °C. Kinetic study is performed using several kinetic models. The carbonation reaction activation energy of CaO in addition of manganese oxide is analyzed. The SEM results showed the surface morphology of pure CaO and CaO-MnO adsorbents. The EDX analysis not only confirmed the elements mass compositions of the CaO and CaO-MnO adsorbents, but also showed the distribution of elements in the adsorbents. For both adsorbents, the compositions were almost same with the theoretical compositions and the distribution of elements were uniform and even throughout the surface. The XRD results was computed and it was found that the mean crystallite size of CaO-MnO adsorbent was smaller than pure CaO adsorbent crystallite size. From the characterization of adsorbents, sol-gel method was proven to be practical in synthesizing CaO-MnO adsorbent. From the CO_2 adsorption study, it was found that the rate of CO_2 adsorption increased with temperature. Besides, CaO-MnO had the highest CO_2 adsorption capacity of 0.4426 mg CO_2/ mg CaO at temperature of 500 °C. At temperature 590 °C, the CO_2 adsorption capacity only around 0.2836 mg CO_2/ mg CaO. This may due to desorption of CO_2. Kinetic model proposed by Wei et al. (2017) was selected to describe the CO_2 adsorption due to its high suitability proven from regression analysis. When compare with other literature results, it was found that the addition of MnO into CaO-based adsorbent will reduce the crystallite size, increase the CO_2 adsorption rate and capacity, as well as reduce the activation energy needed for carbonation reaction.

TABLE OF CONTENTS

LIST OF TABLES

LIST OF FIGURES

LIST OF SYMBOLS / ABBREVIATIONS

2θ	2-Theta, °
A	pre-exponential factor, s^{-1}
E_a	activation energy, kJ/ mol
$FWHM$	Full width at Half Maximum, rad
$g(\alpha)$	integral form of reaction model
k	reaction rate constant, s^{-1}
$k(T)$	temperature-dependent reaction rate constant, min^{-1}
m_f	final mass of adsorbent, mg
m_o	initial mass of adsorbent, mg
m_t	mass of adsorbent at time = t, mg
M_x	molecular weight of species x, mol/g
R	universal gas constant, kJ/ mol K
T	temperature, K
t	time, s
X	conversion
x_{CaO}	mass fraction of CaO adsorbent
X_u	ultimate conversion
α	extent of conversion
θ	Bragg angle, rad
λ	X-ray wavelength, nm
τ	mean crystallite size, nm

CO_2	carbon dioxide
CaO	calcium oxide
MnO	manganese oxide
CaO-MnO	calcium oxide- manganese oxide

LIST OF APPENDICES

CHAPTER 1

INTRODUCTION

1.1 General Introduction

Over the past few decades, global warming had been a concerning issue due to the increase of Earth's average temperature which leads to climate change around the world. With the ever so fast industrial revolution since the mid of 20th century, human activity is likely to be the main cause in the rise of Earth's temperature. For instance, the invention such as steam engine had contributed a lot not only in transportation but also economically. However, such invention comes with a price after a long period of time due to the increase of greenhouse gas emission with the increase usage of it. As shown in Figure 1.1, the carbon dioxide, CO_2 concentration increased significantly.

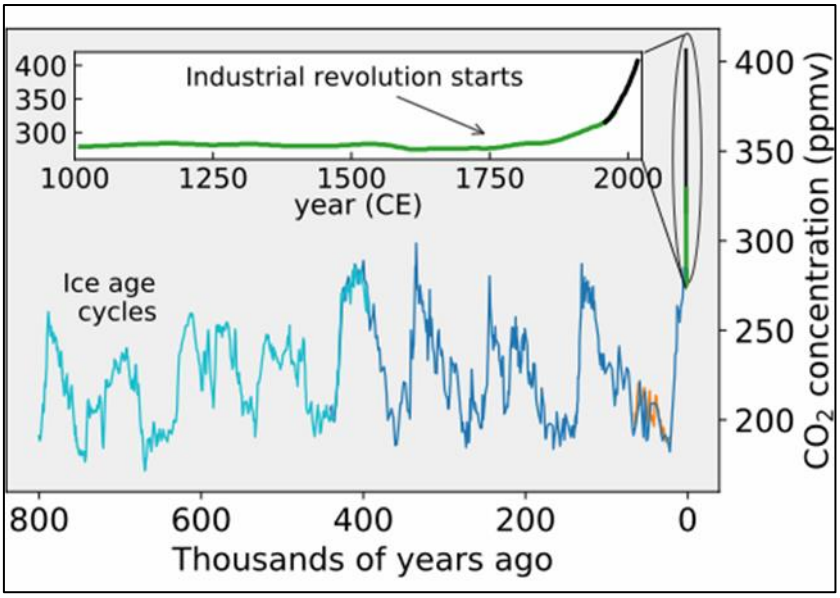

Figure 1.1: Timeline of Concentration of Carbon Dioxide, CO_2 (Nijsse, 2018)

Nowadays, about 80% and more of the world's energy is contributed by fossil fuels and burning of fossil fuel causes the emission of greenhouse gas like carbon dioxide, CO_2 into the atmosphere. CO_2 plays a major role in causing global warming. According to U.S. National Academy of Sciences report in 2008, it was claimed that the global warming was mainly caused by human-induced emission of greenhouse gas. Developed countries like United State of America and China which are one of

the leading leaders in the world, are responsible for the dominant amount of carbon dioxide emission annually.

As to tackle the climate change, 154 countries leaders decided to work together under United Nations Framework Convention on Climate Change (UNFCCC) in 1992. UNFCCC aims to avoid anthropogenic activities which will threaten the environment and cause climate change issue. Greenhouse gas concentration in the atmosphere should be kept at optimum level where the ecosystems will not be troubled in adapting to minor climate change, food production is not in endanger situation and sustainable economy development can be carried out (Rogner, 2007).

For UNFCCC to achieve their aim, a decree was introduced where developed country should spearhead in taking initiative to minimize their respective country emission. This was supported on the basis that the developed country supply as one of the highest cumulation of greenhouse gases in the atmosphere, and their grow to achieve their development needs may increase the emissions of greenhouse gases (Liverman, 2008).

It is necessary to develop technologies that will allow us to utilize the fossil fuels while reducing the emission of greenhouse gases (Abunowara et al., 2012). Carbon dioxide capturing technology may cost a fortune. However, it is undeniable that refining carbon dioxide capturing technology is very important in reducing greenhouse gas emission.

1.2 Importance of the Study

Reducing greenhouse gas such as carbon dioxide is of paramount importance in the tackling global warming. Removal of carbon dioxide with the aid of adsorbent is a viable method in preventing climate change. Among various absorbents that had been studied, calcium oxide-based absorbent is favourable. This is justified by its operating temperature, pressure and carbon dioxide trapping capacity.

Calcium oxide undergoes carbonation process when adsorbing carbon dioxide and calcination process when regenerating the adsorbent.

$$Carbonation: CaO(s) + CO_2(g) \rightarrow CaCO_3(s), \Delta H = -178\ kJ$$

$$Calcination: CaCO_3 \rightarrow CaO + CO_2, \Delta H = 178\ kJ$$

By using calcium oxide as adsorbent material, it is workable in reducing the carbon dioxide emitted into the atmosphere.

The importance of this study is also to determine the effect of transition metal oxide material such as manganese oxide, MnO on the CaO based sorbent performance in CO_2 capture. With the capability of CaO to capture carbon dioxide, a more energy cost efficient way should be investigated, where the efficiency of CaO could be remained high with lower activation temperature for carbonation and calcination.

1.3 Problem Statement

An in-depth research should be done to study the properties of calcium oxide as potential material used as carbon dioxide adsorbent, in order to reduce the emission of greenhouse gas into the atmosphere. Day by day the carbon dioxide emission into the atmosphere increases as the developing countries grow. Thus, sustainable development should be carried out to ensure that the future generation needs can be achieved. The development of calcium oxide based adsorbent which can be considered as green technology also is one of the initiation in reducing the carbon dioxide which leads in climate changes around the world.

Since calcium oxide-based adsorbent possessed such potential, several studies is carried out to enhance the performance for the calcium oxide-based adsorbent. Various research had been carried out to study the factors affecting the efficiency of the calcium oxide based adsorbent. For instance, the performance of CaO was enhanced with addition of catalyst support which reduce the activation energy of the carbonation reaction. Due to the lower activation temperature for the CaO adsorbent to operate in carbonation and calcination cycles, the CaO can capture CO_2 at faster rate. Addition of transition metal oxide caused the CaO-based adsorbent to have higher porosity and surface area for reaction, which hence, increase the efficiency of the CaO adsorbent.

Addition of transition metal oxides into CaO-based adsorbent is proven to be helpful not only in slowing down the degradation of absorbent but also the CO_2 capture performance. The active CaO particle is scattered into porous inert matrix which further supported with anhydrous carbonate mineral or dolomite likes calcium carbonate, $CaCO_3$ and magnesium carbonate, $MgCO_3$. This increases the performance of CaO in CO_2 capture. Transition metal oxide materials like

magnesium oxide, silicon dioxide, cerium (IV) oxide, chromium (III) oxide, copper oxide, cobalt oxide, manganese dioxide, calcium titanate, barium oxide and calcium aluminate, are proven materials used in CaO sorbent synthesis which provide a structure with high porosity. There is still a lot choices of inert material that can be used in synthesizing a CaO sorbent with high CO_2 capture performance and long lasting in high temperature conditions. Manganese (II) oxide is one of the choice which may improve the performance of CaO based sorbent. However, kinetic study should be performed to understand how the adsorbent behave during carbonation process. Therefore, kinetic study is important in investigating the CaO-MnO adsorbent.

1.4 Aims and Objectives

The purpose of this project is to study the potential of CaO-MnO (1:1) as adsorbent in CO_2 capture. This project aim can be achieved with the following objectives:

- To analyse the CO_2 adsorption performance of CaO-MnO adsorbent at different temperatures.
- To characterise pure CaO and CaO-MnO sorbent.
- To perform kinetic study on CO_2 adsorption of CaO-MnO adsorbent.

1.5 Scope and Limitation of the Study

The scopes of this project included the study of the CaO-MnO properties in capturing CO_2. The CO_2 capturing performance of CaO-MnO adsorbent at different carbonation temperature with the aid of Thermal Gravimetric Analyzer (TGA).

The method used to synthesis the CaO-MnO adsorbent and how addition of inert support like MnO to CaO helps in CO_2 capture performance are also studied. The surface morphology of the synthesis CaO and CaO-MnO adsorbent are observed with Scanning Electron Microscope (SEM). Energy Dispersive X-ray (EDX) analysis is done to determine the distribution of the elements present in the CaO and CaO-MnO adsorbents.

A kinetic model is used to determine the activation energy of CaO-MnO adsorbent at different carbonation temperature. The TGA data on CaO-MnO is expressed in term of a linear equation and fit into the kinetic model to determine whether this CaO carbonation reaction operate in the same condition as assumed in

the kinetic model. Then, the activation energy for the Cao-MnO carbonation reaction at different temperature can be determined with Arrhenius equation.

However, there is also limitation to this study, for example, this project only study on the carbonation reaction rather than cyclic reaction (carbonation-calcination). Only activation energy for carbonation of CaO-MnO adsorbent is determined. In this work, the kinetic study is only performed on CO_2 adsorption only.

1.6 Contribution of the Study

This purpose of this project is to find out the most efficient operating condition of the enhanced CaO-MnO adsorbent since this will reduce the emission of carbon dioxide. From this study, the how the CO_2 capturing performance of CaO-MnO adsorbent varies at different carbonation temperatures. This enhancement is important in controlling the greenhouse gas emission at optimum level.

Generally, the calcium oxide based adsorbent has the potential to contribute in managing the emission of greenhouse gases at optimum level. Optimum operating temperature ensure the CaO-MnO adsorbent to function effectively and efficiently while maintaining high durability and performance for carbonation reactions.

1.7 Outline of the Report

In this report, the Chapter 1 is introduction which covers the general global warming issue. Importance of study, problem statement, aims and objectives, scope and limitation of the study, and contribution of study are discussed. Furthermore, Chapter 2 is literature review which reviewed different journals and review papers obtained from various sources which is related to this topic. Important results and findings which helps in this project found by other authors are being paid attention to. Chapter 3 involves methodology and work plan. The materials and equipment used in this project are listed. Flow chart of project methodology, adsorbent performance test method, adsorbent synthesise method, kinetic study and characterisation procedures were proposed. Moreover, Chapter 4 is results and discussion part, which discuss the results obtained from TGA, SEM, XRD and kinetic study of calcium oxide-manganese oxide adsorbent. Finally, in chapter 5, the conclusion of the results and recommendations for future project are included.

CHAPTER 2

LITERATURE REVIEW

2.1 Introduction

The increment of carbon dioxide (CO_2) concentration in the surrounding atmosphere due to the increase of burning of fossil fuel had been a concerning issue nowadays. It was evident that emission of carbon dioxide from fossil fuel burning had contributed to global warming. Fossil fuel which is major energy sources since decades ago until today, will surely continue to release carbon dioxide into the atmosphere even in the future. Global scale CO_2 capture and sequestration (CCS) had been introduced and carefully reviewed.

2.2 Carbon Capture and Sequestration (CCS)

Carbon capture and sequestration (CCS) planning consists of green methods to capture CO_2 from the emission source which then the CO_2 captured is compressed and transported to a safe storage place. Relocation is mainly the idea behind disposing CO_2 in order to nullify the effect of CO_2 on the surrounding environment. For example, the captured CO_2 is stored and injected into geologic or oceanic sinks (Stewart, 2005). CCS determined few major options in relations to CO_2, for example improving the efficiency of production energy, use lower carbon content fuels used by using natural gas and practise the usage of renewable energy likes wind energy and biomass energy. The main problem in executing the CCS plan is where the tasks are a multifaceted problem which needed nationwide awareness and cooperation from multi social likes government, economists, scientists, as well as engineers (Deanna et al., 2010). Besides that, the cost to dispose the captured CO_2 is too high in economic aspect, and the location capacity may be limited, as shown in Table 2.1.

Table 2.1: Estimated World Sink Capacity for CO_2 Disposal Options

Sequestration option	Worldwide capacity (Gigaton carbon, GtC)	Reference
Ocean	1000	Herzog, 2001
Deep saline formations	100-1000	
Depleted oil and gas reservoirs	100	
Coal seams	10-100	
Terrestrial	10	
Utilisation	<1	

It was inevitable that CO_2 capture is considered as another grand barrier in this 21st century. Hence, CaO can be used for CO_2 capture due to its high CO_2 capture capability. CaO is also cheap in term of cost and it is easy to get due to it abundance amount.

2.3 Calcium Oxide based Adsorbent

It is agreeable that calcium oxide-based substances are good choice to be used as CO_2 capture adsorbent. This is due to the properties of calcium oxide (CaO) to absorb CO_2 at high rate and CaO has high CO_2 capture capacity. CaO also cost low in the current market. When CaO capture CO_2 at its high carbonation temperature around 700 ℃, numerous amounts of energy from the reaction can be retrieved as high-quality heat efficiently (Florin, 2008). CaO-based material as adsorbent is better than other materials which operate at lower temperature due to high heat recovery possessed by the CaO-based material (Romano, 2009). Yet, carbonation of CaO and calcination of $CaCO_3$ are not complete or reversible (Grasa, 2006). Severe sintering of adsorbent is prone to be happen and cause the CO_2 capture capacity to decline. This is because carbonation process is highly exothermic.

$$CaO + CO_2 \rightarrow CaCO_3, \Delta H = -177.8\, kJ \quad (2.1)$$

Moreover, the high-volume change of CaO to $CaCO_3$ reduces the distance between the adsorbent particle during carbonation process. Tammann temperature or the

highest temperature of a material can withstand before prone to sintering, of $CaCO_3$ is 533 ℃ which is lower than the carbonation temperatures (Lu et al., 2009).

2.4 Development of CaO-based Sorbent Synthesis

Improving the performance of CaO-based CO_2 adsorbent had been a focused subject in researches for ways to prevent the loss of CO_2 capture capacity problem.

2.4.1 Sintering Resistant Calcium Precursors

Potential of calcium precursor is worthy to be evaluated because some calcium precursor can be utilized to form sintering-resistant adsorbent. The calcium precursor can also increase the selectivity of CaO which at the same time enhance the not only the reactivity of CaO but also the carbonation-calcination cycle performance of the synthesised CaO sorbent. High availability and low-cost materials like hydrated lime ($Ca(OH)_2$), limestone ($CaCO_3$) and lime (CaO), had been considered a good option in the use for CO_2 capture purposes. Calcium precursor like calcium nitrate ($Ca(NO_3)_2$) had no CO_2 capture properties and prone to sintering at calcination stage (Lu et al., 2006). Thus, calcium nitrate is not suitable to be utilized in this case. Nano-sized $CaO/CaCO_3$, organometallic precursors and precipitated $CaCO_3$ (PCC) had the best performance in sintering resistant.

2.4.2 Doping

The surface grain degradation of CaO and calcium precursor sorbent can be impeded or slow down with pre-treatment method like doping (Salvador et al.,2003). One of proven doping method in increasing the carbon dioxide capture capacity of limestone in fluidized bed reactors is sodium salts likes sodium carbonate (Na_2CO_3). In doping of Na_2CO_3 on the CaO, the porosity of CaO structure is rearranged by the sodium into a preferable pore dispersion for gas contact. Sodium chloride (NaCl) analysed in Thermal Gravimetric Analysis (TGA) equipment appeared to help in enhancing the cyclic ability of the sorbent. However, NaCl and sodium carbonate (Na_2CO_3) are tested and found not that effective in enhancing the cyclic performance in fluidized bed combustors condition. Doping of Na_2CO_3 and NaCl is found to notably reduce the capacity of capture in fluidized bed combustors conditions. In this case, the enhancement of carbon dioxide capturing ability may also due to hydration of the

adsorbent as aqueous component also used in synthesising the sorbent with doping method.

2.4.3 CaO Particle Dispersion in Inert Matrix

Mixing of CaO particle in inert matrix had been seen as another promising synthesis method. Various research had been done to analyse the performance of CaO in carbon dioxide capture with addition of inert solid matrix. The active CaO particle is scattered into porous inert matrix which further supported with anhydrous carbonate mineral or dolomite likes calcium carbonate, $CaCO_3$ and magnesium carbonate, $MgCO_3$. This not only increase the performance of CaO in CO_2 capture but also increase the heat sintering resistance of the CaO absorbent. The decomposition of $MgCO_3$ to MgO Inert support materials like magnesium oxide, silicon dioxide, cerium(IV) oxide, chromium(III) oxide, copper oxide, cobalt oxide, manganese dioxide, calcium titanate, barium oxide and calcium aluminate, are proven materials used in CaO sorbent synthesis which not only provide a structure with high porosity but also high heat sintering resistance. Although Na_2CO_3 helps in enhancing the sorbent performance, however the Na_2CO_3 price may limit the usage of the chemical component in the industry. Besides that, agglomeration and fouling prone to happen in this case.

Other than adding metal salts to improve CaO performance, doping mixture can also be mixed to CaO or $CaCO_3$ too. According to Roesch et al. research, CaO/Cs_2O sorbent can be formed by infusing CaO into CsOH solution. This CaO/Cs_2O sorbent had enhanced carbon dioxide capture performance. Furthermore, Li et al. research used $CaCO_3$ with addition of 0.8 wt% $KMnO_4$ solution to maintain high conversion even after 100 cycles of carbonation and calcination reaction.

2.4.4 Promising Synthesis Method

From Table 2.2, it was shown that various methods were used to synthesizing various types of calcium-based adsorbent. Some of the calcium-based precursors show some promising results. For example, precursors synthesis by Li et al. (2010) with doping and mixing method, showed that the precursor last for 100 and above cycles of carbonation and calcination while maintaining around 0.4 g/g capacity.

Table 2.2: Calcium-based Adsorbent Performance with Different Synthesis Method

Method	Precursors	Number of cycles	Last cycle capacity (g/g)	Reference
Doping	$CaCO_3$, 20 wt% NaCl solution	14	0.40	Salvador et al., 2003
Doping	$CaCO_3$, 20 wt % $KMnO_4$ solution	100	0.44	Li et al., 2010
Mixing	Nano-$CaCO_3$, TiO_2	40	0.2365	Wu and Zhu, 2010
Mixing	CaO, $Al(NO_3)_3$ solution	50	0.39	Li et al., 2006
Mixing	Calcined calcium acetate, $Al(NO_3)_3$ solution	45	0.30	Martavaltzi and Lemonidou, 2008
Mixing	Calcium acetate, prepared SBA-15	40	0.24	Huang et al.,2010
Mixing	Calcium acetate, magnesium oxalate	132	0.43	Li et al., 2010
Mixing	Calcium D-gluconate solution, magnesium D-gluconate solution	24	0.38	Liu et al., 2010
Wet impregnation	$CaCl_2$, porous γ-aluminium	9	0.03	Feng et al., 2006
Physical mixing	$CaCO_3$, SiO_2	13	0.21	Wang et al., 2008
Sol-gel combustion synthesis	$Ca(NO_3)_2$ solution, $La(NO_3)_3$ solution	11	0.58	Luo et al., 2011
Sol-gel combustion synthesis	$Ca(NO_3)_2$ solution, $La(NO_3)_3$ solution	11	0.456	Luo et al., 2011

Table 2.2 (Continued)

Mixed precipitation	$Ca(OH)_2$, $al(NO_3)_3 \cdot 9H_2O$	30	0.228	Florin and Fennel, 2011
Mixing and pelletization	Calcined limestone, calcium aluminate cement	1000	0.158	Manovic and Anthony, 2009

2.5 Sol-gel Combustion Method

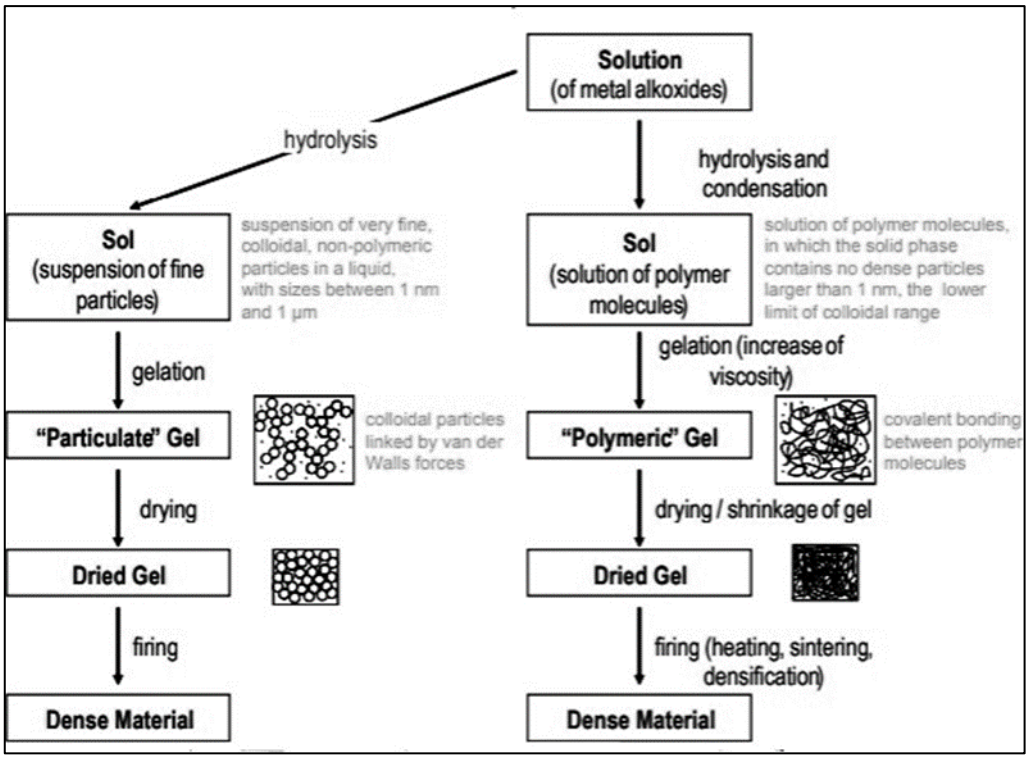

Figure 2.1: Schematic Diagram on Preparation for Sol-gel Method (Marques, 2007)

Nanomaterial is normally prepared with sol-gel combustion method as this method has better structure control when synthesising. From Table 2.2 above, Luo et.al synthesised calcium-based adsorbent with sol-gel combustion method. Firstly, the sol and gel is prepared by mixing $La(NO_3)_3 \cdot 6H_2O$ with $Ca(NO_3) \cdot 24H_2O$ in distilled water. $Al(NO_3)_3 \cdot 9H_2O$ can be used to replace $La(NO_3)_3 \cdot 6H_2O$. To produce the sol, the mixed mixture is then added with citric acid and further stirred. Then the mixture is dried for a period of 7 hours at temperature of 80 ℃. The produced sol is then left

in room temperature to turns in to wet gel. Dry gel is then obtained by heating the wet gel at temperature of 600 ℃. From many past research, it was found that inert materials like La_2O_3 and $Ca_{12}Al_{14}O_{33}$ can be used in producing promoted sorbent which had high CO_2 capture performance.

2.5.1 Advantages of Sol-gel Combustion Method

Sol-gel combustion synthesis method is known for its versatility as it has better control on the porosity and particle size. This method is famous for preparation of nanomaterials and organic components into sol-gel derived oxides. Sol-gel method also has better homogeneity or in another word, high purity, as it is mixed at molecular level. This synthesis method can also be conducted at lower temperature where melting temperature no need to be achieved. Less energy is required for this synthesis method at the low temperature. This synthesis method can used and produced wide range of components. All oxides components and some non-oxides components too can be fabricated using this synthesis method. Organic-inorganic sorbent can also be made with this method. In this sol-gel synthesising process, there is no expensive or particular laboratory equipment required for synthesising.

2.6 Shrinking Core Model

The condition where consumption of solid particle by dissolution or reaction can be explained with the Shrinking Core Model (SCM). The loss of the solid particle as time goes is known as shrinking. The solid reactant particle does not disappear or appear but converted from one reactant to another product in the reactions. This model has wide range of application from pharmacokinetics to formation of CO_2 from oxygen and carbon reaction. For example, SCM can be used to describe the carbonation and calcination of calcium-based sorbent too (Fogler, 2015).

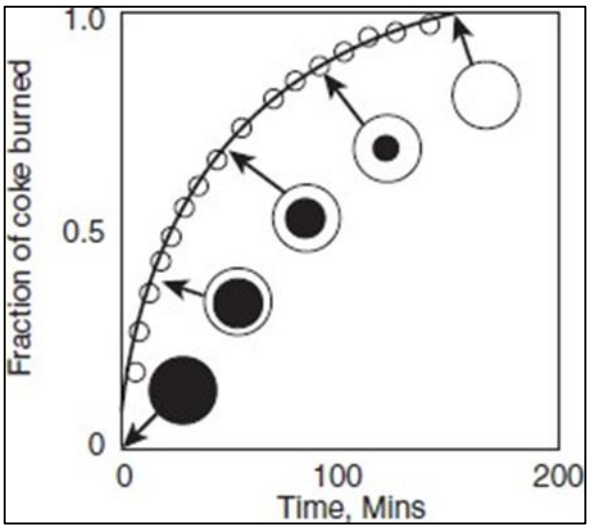

Figure 2.2: Regeneration of Carbon Particle at Different Time (Richardson, 1972)

In Figure 2.2, it was shown the catalyst regeneration by burning the carbon layer in the presence of oxygen. The amount of carbon layer on the catalyst reduced as the time goes. The reaction slowly takes place from the surface of the catalyst to the core of the particle. As the regeneration reaction proceed, it can be observed that the carbon layer started to reduce slowly from the surface of the particle then forming a carbon core.

2.6.1 Shrinking Core Model Assumption

According to Safari et al. (2009), few assumptions are made in shrinking core model where the particle reacting in the reaction is in isothermal conditions. Furthermore, the size of particle is assumed the same throughout the reaction. The durability of the particle remains high where the particle is assumed will not break apart due to thermal stress. The reactant particle can be assumed as a single particle which the condition can be satisfy as same as batch reactor conditions.

2.6.2 Diffusion-limited and Reaction-limited Stage

From rate of reaction profile, it can be observed that a reaction constitutes specific regime or region with different reaction rate. The regimes consist of diffusion-limited stage, transition phase and reaction-limited stage. At diffusion-limited stage, the reaction rate is much higher than the rate diffusion. The reaction rate is limited by the diffusion of the gas molecule to the solid active site. At transition phase, the rate of

reaction slowly reduces as the amount of available active site reduce. At reaction-limited stage, the rate of the reaction is limited by the reaction rate due to reactant or active site depletion.

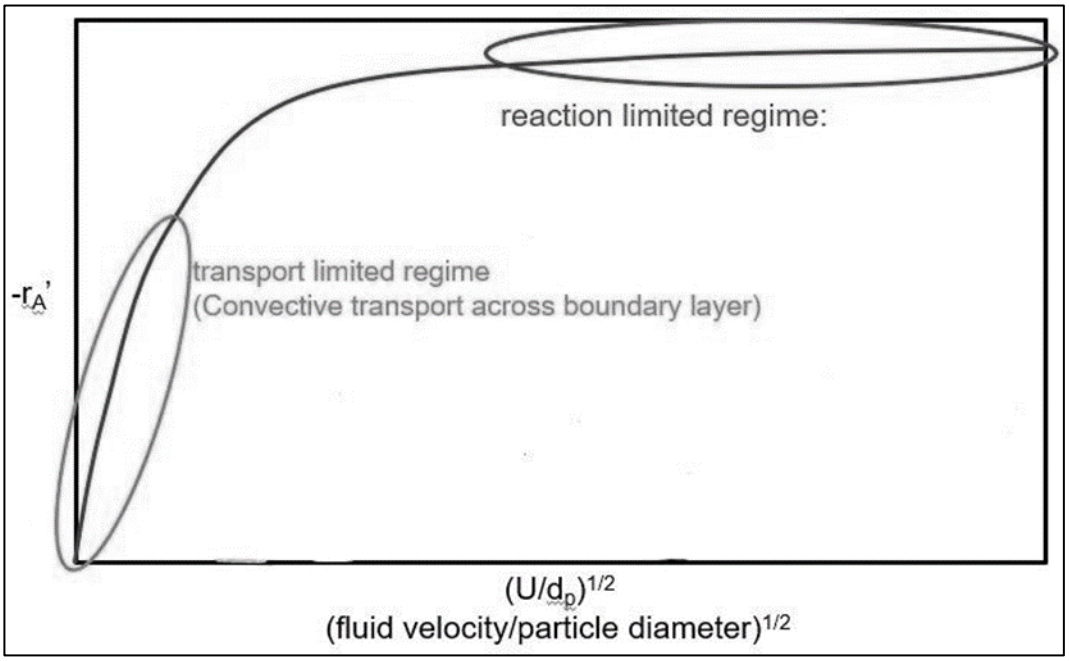

Figure 2.3: The Diffusion and Reaction Limited Region of Reaction (Fogler, 2016)

According to Kazi et al. (2014), the reaction of CaO in CO_2 capture was also consisting of three reaction rate regimes. This includes a rapid rate of reaction at diffusion-limiting stage, followed by a slower reaction rate at transition stage and finally the slowest reaction rate at reaction-limiting stage where the CO_2 diffusion through the $CaCO_3$ layered formed to reach the fresh CaO is hindered.

2.7 Kinetic Study

The kinetic study on the performance of CaO-based adsorbent in CO_2 capture can be described with the aid of kinetic models from mathematical derivation. Throughout the years, various kinetics model derived from different models, principles and assumptions were performed in order to find the best kinetic model to describe certain process, for example gas-solid reaction between CO_2 and CaO-based adsorbent. The kinetic study not only provides better understanding on certain reaction process but also able to provide the knowledge to improve the performance of the reaction.

2.7.1 CO_2 Adsorption and Desorption Analysis Method

According to Wei et al. (2017), the isothermal kinetic process of the CO_2 adsorption can be explained with the reaction models in the Table 2.3.

Table 2.3: Reaction Model for CO_2 Adsorption and Desorption

Reaction Model	g(α)
Zero-order (R1)	α
First-order (A1)	-ln(1-α)
Second-order (F2)	$(1-\alpha)^{-1}-1$
Third-order (F3)	$(1/2)[(1-\alpha)^{-2}-1]$
One-dimensional diffusion (D1)	α^2
Two-dimensional diffusion (D2)	(1-α)ln(1-α) +α
Three-dimensional diffusion Jander equation (D3)	$[1-(1-\alpha)^{-1/3}]^2$
Three-dimensional diffusion Ginstling-Brounshtein (D4)	$(1-2\alpha/3)- (1-\alpha)^{-2/3}$

For this kinetic model analysis, the ratio between the mass change of adsorbent to the initial mass of adsorbent is defined as extend of conversion, α.

$$\alpha = \frac{m_o - m_t}{m_o - m_f} \tag{2.2}$$

where

α = extend of conversion

m_o = initial mass of adsorbent

m_t = mass of adsorbent at time = t

m_f = final mass of adsorbent

The CO_2 adsorption and desorption process can be explained by the Eq. 2.3.

$$\frac{d\alpha}{dt} = k(T)f(\alpha) \tag{2.3}$$

$$\frac{d\alpha}{f(\alpha)} = k(T)\, dt \tag{2.4}$$

$$\int_0^{\alpha} \frac{d\alpha}{f(\alpha)} = g(\alpha) = \int_0^{t} k(T)\, dt \tag{2.5}$$

By integration method, integral form of reaction model, $g(\alpha)$ to describe the CO_2 adsorption and desorption process can be obtained. The $g(\alpha)$ can be relate to the reaction rate constant which dependant on the temperature as shown in the Eq. 2.6 The kinetic parameter can also be determined by data fitting where the Eq. 2.6 expressed in linear form as shown below:

$$g(\alpha) = k(T)t \tag{2.6}$$

where

$g(\alpha)$ = reaction model integral form

$k(T)$ = rate constant function, min^{-1}

t = time, min

2.7.2 CaO Carbonation Analysis Method

In a research conducted by Lee (2003), a simpler version of model was developed to explain the CaO carbonation reaction at high CO_2 concentration (Nikulshina, 2006). From the graphs above, it can be observed that the carbonation reaction rate is high at low conversion stage, and the initial carbonation reaction rate vary at different temperature. When the ultimate conversion, X^u is achieved, there is no more conversion reaction occur in the system. The constant k is used to denote the rate of CaO carbonation. The rate of carbonation conversion for the CaO carbonation can be shown as:

$$\frac{dX}{dt} = k\left(1 - \frac{X}{X_U}\right)^n \tag{2.7}$$

When the CaO carbonation reaction started, the conversion at initial stage can be neglected due to the low conversion. In this case, the conversion rate is considered dependent on k. Hence, on the surface of the CaO particle, k can be considered as the constant of intrinsic chemical reaction rate constant in unit of time^{-1} (t^{-1}). The conversion rate reduced as the conversion increases, as shown in the term; $(1-X/X_u)^n$. At $X = X^u$, the conversion rate is zero. To relate the conversion with time, the parameter n value can be substitute with 1 and 2 for integration of Eq. 2.7. Then, the conversion as an explicit function of time can be obtained as shown below:

$$X = X_u \left[1 - exp\left(-\frac{k}{X_U} t\right)\right] \tag{2.8}$$

$$X = \frac{X_u t}{(X_u/k) + t} \tag{2.9}$$

Constant b which denotes the time taken by the reaction to achieve half of the ultimate conversion is added, at t = b, $X = X_u/2$. After substitute the relationship into Eq. 2.9, the ultimate conversion of CaO can be illustrated as:

$$X_u = kb \tag{2.10}$$

Substituting Eq. 2.10 to Eq. 2.9 produced another equation for conversion in term of time, as shown below:

$$X = \frac{kbt}{b + t} \tag{2.11}$$

The rate of disappearance of CO_2 by CaO carbonation reaction can be explained in Eq. 2.12 below, assuming there is no external mass transfer limitation of CO_2 to CaO particles.

$$r_{CO_2} = \frac{1}{M_{CaO}}\left(\frac{dX}{dt}\right) \tag{2.12}$$

Where r_{co2} is the molar rate of CO_2 disappearance per unit mass of CaO, and M_{CaO} is the molecular weight of CaO. Gas term regarding the concentration of CO_2 gas is not found in the rate of disappearance of CO_2 because the CO_2 partial pressures affect very insignificantly compared to the rate of CaO carbonation at early phase of carbonation. Besides that, the rate of reaction at reaction limiting stage was independent of CO_2 partial pressure.

The kinetic parameter can be determined by data fitting where the Eq. 2.11 expressed in linear form as shown below:

$$\frac{1}{X} = \frac{1}{k}\left(\frac{1}{t}\right) + \frac{1}{kb} \tag{2.13}$$

2.8 Arrhenius Equation

Rate of reaction which is dependent to temperature can be explained with the Arrhenius equation. In the Arrhenius equation, the reaction rate constant (k) is shown dependent to the temperature of the reaction (T), pre-exponential factor (A) and the reaction activation energy (E_a).

$$k = Ae^{\frac{-Ea}{RT}} \tag{2.14}$$

Arrhenius plot which is in linear form can be obtained by multiplying both side with natural logarithm.

$$ln(k) = ln(A) + ln\left(e^{\frac{-Ea}{RT}}\right) \tag{2.15}$$

$$ln(k) = ln(A) - \frac{Ea}{R}\left(\frac{1}{T}\right) \tag{2.16}$$

The equation has the same linear form as equation of a straight line.

$$y = mx + c \tag{2.17}$$

With the aid of graph, the activation energy of the reaction can be determined.

CHAPTER 3

METHODOLOGY AND WORK PLAN

3.1 Introduction

Before conducting this research to study the properties of CaO-MnO adsorbent in CO_2 capture, the materials, equipments and procedures are planned to ensure the aim and objectives are achieved.

3.1.1 Materials and Chemicals

The material and chemical used in this project was shown in Table 3.1.

Table 3.1: List of Material and Chemical Used

Chemicals	Specification	Quantity
Calcium nitrate tetrahydrate, $Ca(NO_3)_2{\cdot}4H_2O$	Merck >99%	5.9038 g
Manganese(II) nitrate hexahydrate, $Mn(NO_3)_2{\cdot}6H_2O$	Merck >99%	6.2753 g
Citric acid monohydrate, $C_6H_8O_7{\cdot}H_2O$	Merck >95%	15.7605 g
Distilled Water, H_2O		50 ml

3.1.2 Apparatus and Equipment

The apparatus and equipment used in this project was shown in Table 3.2. The instrument used in this project was shown in Table 3.3.

Table 3.2: List of Apparatus and Equipment Used

Apparatus/ Equipment	Purpose
Magnetic Hot Plate Stirrer	To heat and stir the mixture until dry during adsorbent synthesise
Oven	To further dry the wet gel mixture
Programmable Furnace	To calcinate the dry gel into powder

Table 3.3: List of Instrument Used

Instrument	Purpose
Thermal Gravimetric Analyser (TGA)	To study the CO_2 adsorption of the adsorbent
X-ray Diffraction (XRD)	To analyse the crystallite structure
Scanning Electron Microscope- Energy Dispersive X-ray Analyser (SEM- EDX)	To study the surface morphology and the surface elements composition of the adsorbent

3.2 Research Flow Diagram

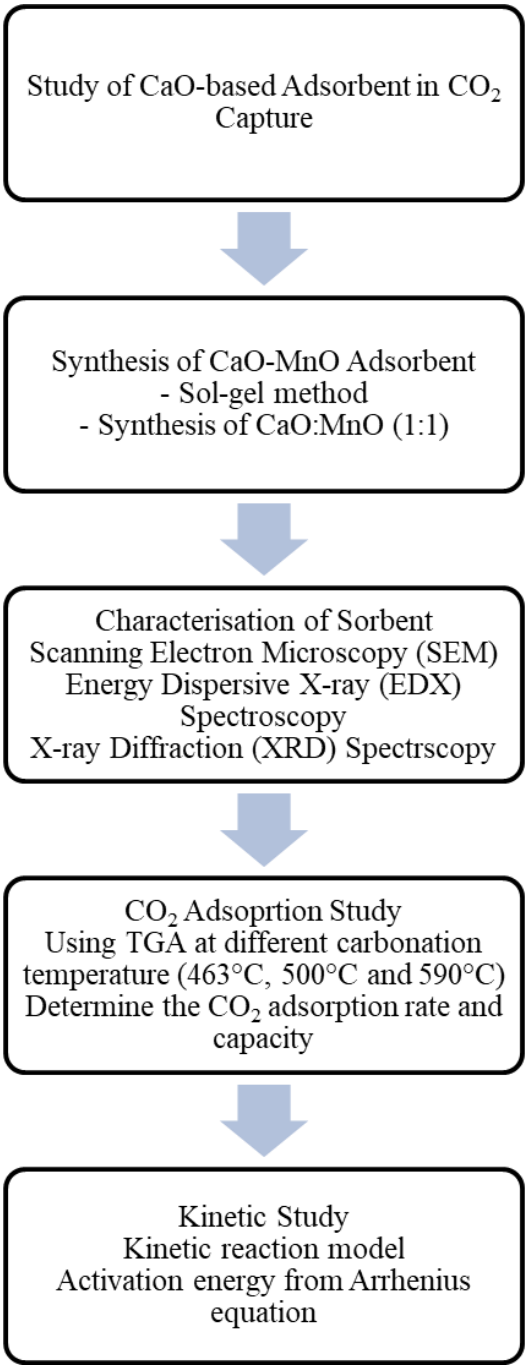

Figure 3.1: Methodology Research Flow Diagram

The study of CaO-based adsorbent in CO_2 capture was started with the synthesis of CaO-MnO (1:1) adsorbent with sol-gel method. Then, characterisation of adsorbent by SEM, EDX and XRD analysis were performed on the adsorbent. CO_2 adsorption study was performed in TGA at different temperature to determine the synthesised adsorbent adsorption rate and capacity. From the data obtained from TGA analysis, kinetic study was performed to verify which kinetic models were the best to describe

the CaO-based adsorbent CO_2 capture process. With Arrhenius equation, activation energy of the CaO-MnO adsorbent in CO_2 adsorption reaction was determined.

3.3 Synthesis of CaO-MnO Adsorbent

The CaO-MnO adsorbent was synthesised with sol-gel method as this method has better structure control. In order to synthesis CaO-MnO adsorbent, the sol and gel were prepared by mixing calcium nitrate tetrahydrate and manganese(II) nitrate hydrate at 1:1 molar ratio. Then, citric acid was added into the mixture at the molar ratio of 1:3 (citric acid: precursor). Next, 50 ml of distilled water was added into the powder mixture. The mixture was then heated to about 90℃ and stirred vigorously using hot plate with magnetic stirrer. The mixture was heated until a low water gel-like consistency obtained. The wet gel was then transferred into a crucible and further dried in oven for 3 hours at 100 °C. Then, the dry gel was then placed into programmable furnace to be calcinate at 700 ℃ for 4 hours. The powder products were then left to cool before stored into a storage bottle. Parafilm was used to seal the bottle to avoid further contamination of the adsorbent.

3.4 Characterisation of Sorbent

Characterisation on synthesised CaO-MnO adsorbent was performed to have a better understanding on the synthesised adsorbent in term of the physical and chemical properties of the adsorbent.

3.4.1 Scanning Electron Microscopy (SEM)

SEM was used to study the surface morphology of the adsorbents sample. By using SEM, the surface morphology of pure CaO and synthesised CaO-MnO adsorbent can be examined. In this experiment, Hitachi Scanning Electron Microscope S-3400N was used and the powder sample in the sample holder was coated with a thin gold layer to increase conductivity, before being placed into the SEM. The adsorbent sample was scanned at 15.0kV and magnification of 15,000x. Few SEM images were captured, and the clearest SEM images were then used to study the surface morphology of the adsorbents.

3.4.2 Energy Dispersive X-ray Analyzer (EDX)

Along with the SEM test, EDX test was carried out to analyse the weight composition of elements in the adsorbents. EDX can also show the distribution of

each elements in the adsorbents. From the weight composition and distribution of the elements, the feasibility of synthesis method can verify.

3.4.3 X-ray Diffraction (XRD) Spectroscopy

XRD is rapid analytical method to identify the crystal structure crystalline materials. In this experiment, XRD test was carried out to identify the component present in both pure CaO adsorbent and MnO-added CaO adsorbent. The available XRD equipment in the laboratory is Shidmazu XRD-6000. The XRD uses Cu K-α for the scanning X-ray laser which uses 40.0 kV and 30.0 mA. In the XRD test, the sample was scanned from diffraction angle, 2θ = 20° to 80° at the scan speed of 1.2 °/min. By using Scherrer equation in Eq. 3.1, the mean crystallite size can be calculated. The mean crystallite size of 3 strongest peaks was calculated to obtain an average crystallite size of the adsorbent.

$$\tau = \frac{0.94\lambda}{FWHM \times Cos\,\theta} \tag{3.1}$$

where

τ = Mean crystallite size, nm

λ = X-ray weavelength (0.154056 nm, Cu K-α)

$FWHM$ = Full Width at Half Maximum, rad

θ = Bragg angle, rad

3.5 CO_2 Adsorption Performance Study

The CaO carbonation process at temperature of 463 ℃, 500 ℃ and 590 ℃ can be carry out in Thermogravimetric Analyzer (TGA). The temperature program set in the TGA was as shown below:

1. Heat from 50 ℃ to 700 ℃ at 10.00 ℃/min.
2. Hold for 20 min at 700 ℃.
3. Cool from 700 ℃ to 500 ℃ at 20 ℃/min.
4. Hold for 60 min at 500 ℃.

Steps 1 and 2 were used as adsorbent pre-treatment to remove any $CaCO_3$ layer. During this pre-treatment phase, nitrogen gas was passed through the adsorbent sample at the flow rate of 20 cm^3/min. After the end of Step 2, the

temperature was reduced at the rate of 20.00 °C/min until desired experimental temperature was achieved. When the desired experimental temperature was achieved, the temperature was maintained. Then, CO_2 gas was passed through the adsorbent sample at flow rate of 20 ccm/min for 60 min. The procedures were repeated by changing the desired temperature to carry out the carbonation process.

3.5.1 CO_2 Adsorption Capacity and Rate

From the TGA test, the weight change of the adsorbent throughout the 60 minutes duration can be obtained. The TGA results can be used to calculate the CO_2 adsorption capacity and CO_2 adsorption rate of the adsorbent.

$$CO_2\ adsorption\ capacity = \frac{m_t - m_o}{m_o \times x_{CaO}} \tag{3.2}$$

where

m_o = initial mass of adsorbent, mg (t = 0)

m_t = mass of adsorbent at time t, mg

x_{CaO} = mass fraction of CaO present in adsorbent

The CO_2 adsorption capacity indicates the mass of CO_2 captured per unit mass of CaO in the adsorbent. The unit for CO_2 adsorption capacity shown in Eq. 3.2 was mg CO_2/ mg CaO. The CO_2 adsorption rate shows the mass of CO_2 captured per unit mass of CaO in the adsorbent and time. The CO_2 adsorption rate which can be expressed in the unit of mg CO_2/ mg CaO min was shown in Eq. 3.3:

$$CO_2\ adsorption\ rate = \frac{m_t - m_o}{m_o \times x_{CaO} \times t} \tag{3.3}$$

where

m_o = initial mass of adsorbent, mg (t = 0)

m_t = mass of adsorbent at time t, mg

x_{CaO} = mass fraction of CaO present in adsorbent

t = time, min

3.6 Kinetic Study

The kinetic study on the performance of CaO-based adsorbent in CO_2 capture can be described with the aid of kinetic models derived. In this experiment, two sets of kinetic models were used to determine which kinetic models were more suitable and accurate to describe the CaO carbonation process.

3.6.1 CO_2 Adsorption and Desorption Kinetic Model

According to Wei et al. (2017), the isothermal kinetic process of the CO_2 adsorption can be explained with the equation shown in Eq.3.4.

$$g(\alpha) = k(T)t \tag{3.4}$$

where

$g(\alpha)$ = reaction model integral form

$k(T)$ = rate constant function, min^{-1}

t = time, min

Eq. 3.4 shows linear relationship between the integrated reaction model, g(α) with time, t. Rate of reaction of a process can be divided into three stages which is diffusion-limiting stage, transition phase and reaction-limiting stage. Rate of reaction was the highest during diffusion-limiting stage. The rate of reaction decreases as it enters transition phase and in reaction-limiting stage, the rate of reaction was the slowest. In order to determine the best reaction model to describe the CO_2 adsorption process at each stage, regression analysis can be done to the g(α) against t relationship. From the least squares regression line, the most accurate and likely reaction model function to describe the process at each stage can be determined. Least squares regression line which had the R^2 value nearest to 1 indicates the results fits the model the best. The reaction rate constant, k can be determined by referring to the slope of the linear squares regression line.

Regression analysis was done to measured how close the results fitted to the proposed kinetic model. If the R^2=1, then the kinetic model best described all the variability of the TGA result data. Then, the reaction rate constant, k for both diffusion limited stage and reaction limited stage can be determined from the graph.

Table 3.4: Reaction Model for Each Stage (Wei et al. 2017)

Rate-Limiting Stage	Reaction Model	g(α)
Diffusion-limited Stage	Zero-order (R1)	α
	First-order (A1)	$-\ln(1-\alpha)$
	Second-order (F2)	$(1-\alpha)^{-1}-1$
	Third-order (F3)	$(1/2)[(1-\alpha)^{-2}-1]$
Reaction-limited Stage and Transition Phase	One-dimensional diffusion (D1)	α^2
	Two-dimensional diffusion (D2)	$(1-\alpha)\ln(1-\alpha)+\alpha$
	Three-dimensional diffusion Jander equation (D3)	$[1-(1-\alpha)^{-1/3}]^2$
	Three-dimensional diffusion Ginstling-Brounshtein (D4)	$(1-2\alpha/3)-(1-\alpha)^{-2/3}$

3.6.2 Lee CaO Carbonation Kinetic Model

For this kinetic model, the CaO weight change results from TGA was firstly used to calculate the conversion of the CaO. Then, the conversion values were substituted into Eq. 2.13 to plot a linear graph of (1/X) against time (1/t).

Regression analysis was done on the graph plotted from the TGA results. The graph of (1/X) against time (1/t) is measured how close the results fitted to the kinetic model in Eq. 2.13 If the R^2= 1, then the kinetic model described all the suitability of the TGA result data with the kinetic model. Then, the reaction rate constant, k for the CO_2 adsorption reaction can be determine from the gradient of the least square regression line.

3.6.3 Arrhenius Plot

The determined reaction rate constant, k obtained from the gradient of the least squares regression line for carbonation temperature 463 °C, 500 °C and 590°C of each best fit model were substituted in to Arrhenius equation. From the Arrhenius plot, the activation energy, E_a and pre-exponential factor, A can be calculated.

CHAPTER 4

RESULTS AND DISCUSSIONS

4.1 Characterisation of Adsorbent

Characterisation on synthesised CaO-MnO adsorbent was performed to have a better understanding on the synthesised adsorbent in term of the physical and chemical properties of the adsorbent.

4.1.1 Scanning Electron Microscopy (SEM)

SEM was used to analyse the surface morphology of synthesized CaO and CaO-MnO adsorbent. The SEM images at different spots were tabulated in Table 4.1.

Table 4.1: SEM Images of CaO and CaO-MnO Adsorbent

CaO	CaO-MnO
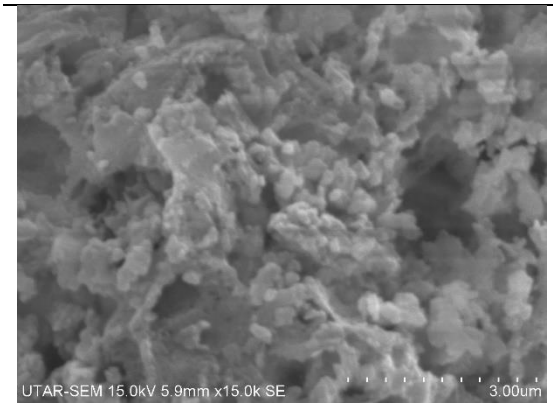	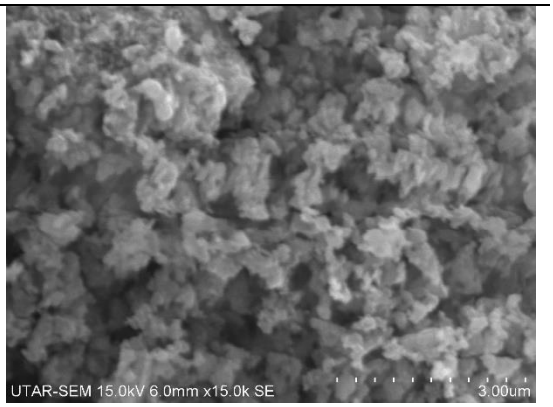
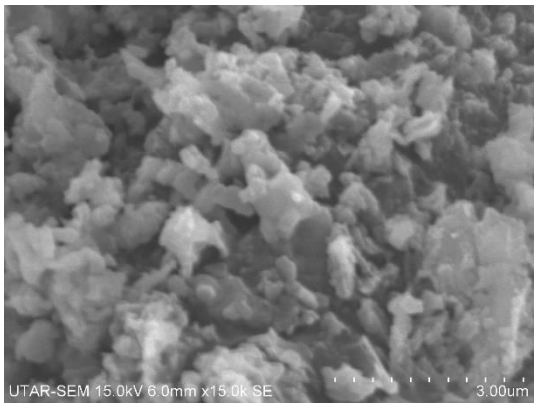	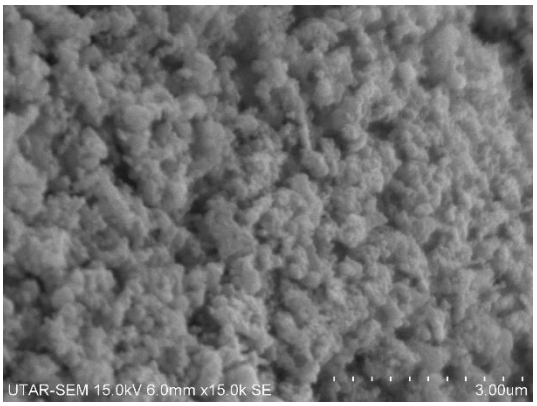

The SEM images above showed the surface morphology of CaO and CaO-MnO adsorbents after synthesizing through sol-gel method. CaO surface under the SEM exhibited uneven and porous surface. On the CaO sample surface, there is also

distribution of amorphous-like particle. It was observed that the shape of the crystallites was round, and their edges were not well defined. The CaO adsorbent sample consists of continuous round structure which formed by attached particle. The particle size distribution of CaO sample was broad. It was evident that there was also formation of well-shaped particle lumps which can be observed in CaO sample SEM images. According to Galvan-Ruiz (2009), those lumps were produced during synthesising process where the dry slaked lime reacted with water in the atmosphere to produce calcium hydroxide, $Ca(OH)_2$.The $Ca(OH)_2$ formed then spontaneously react with CO_2 to formed a more stable compound which is $CaCO_3$. Therefore, this explained the formation of well-shaped lumps on the CaO sample.

The particle size become finer or smaller after addition of MnO into CaO adsorbent. The adsorbent became more porous compared to CaO adsorbent. The high porosity distributed the active sites so that the active sites were more easily exposed in capturing CO_2. Therefore, the CO_2 capture capacity and CO_2 capture rate can be increased with the addition of MnO.

4.1.2 Energy-dispersive X-ray Spectroscopy (EDX)

EDX was used to determine the surface composition of CaO and CaO-MnO adsorbents. From the EDX test, the weight percentage of different elements in the adsorbents were determined. The results obtained from EDX test were tabulated in Table 4.2 and Table 4.3.

The actual weight fraction of each elements was compared with the calculated theoretical weight fraction in Appendix C. CaO can easily undergoes carbonation reaction during and after synthesising process. The weight if $CaCO_3$ was taken in account when calculating the theoretical weight fraction due to high possibility of $CaCO_3$ formation.

Table 4.2: EDX Element Composition of CaO Adsorbent

Elements	**Weight Percentage (wt %)**		
	C	**O**	**Ca**
Spot 1	26.90	45.91	27.19
Spot 2	26.65	43.74	29.61
Spot 3	15.85	43.73	40.42

Table 4.2 (Continued)

Spot 4	12.05	42.75	45.20
Spot 5	14.40	42.86	42.73
Average Weight Percentage	19.17	43.80	37.03
Average Weight Fraction	0.1917	0.4380	0.3703
Theoretical Weight Fraction	0.0769	0.4098	0.5133

Table 4.3: EDX Element Composition of CaO-MnO Adsorbent

Elements	**Weight Percentage (wt %)**			
	C	**O**	**Ca**	**Mn**
Spot 1	21.79	31.24	24.92	22.05
Spot 2	15.15	35.25	28.93	20.66
Spot 3	21.66	32.34	24.79	21.22
Spot 4	4.70	30.91	33.96	30.42
Spot 5	24.18	32.50	26.32	17.00
Spot 6	27.43	33.48	21.26	17.83
Average Weight Percentage	19.15	32.62	26.70	21.53
Average Weight Fraction	0.1915	0.3262	0.2670	0.2153
Theoretical Weight Fraction	0.0529	0.3522	0.3530	0.2419

According to Table 4.2 and Table 4.3, it was observed that the actual weight fraction is slightly different from the theoretical weight fraction. For carbon, the actual weight fraction was higher than theoretical weight fraction value. This may happen due to the carbon tape used to hold the sample for EDX. Besides, the high carbon weight fraction may also due to the formation of $CaCO_3$ from CaO. There was indeed CaO carbonation occurred on the CaO sample as it was evident that the oxide weight fraction is higher than calcium despite oxide having lower molar weight. For the CaO-MnO sample, there was CaO carbonation too as the oxide weight fraction was higher compared to elements like calcium and manganese which had higher molar weight.

The EDX data for CaO-MnO sample showed that the actual and theoretical weight fraction were almost the same. Therefore, the sol-gel method used to

synthesis the CaO-MnO adsorbent was successful to produce adsorbent with correct respective chemical composition and well distribution of each elements.

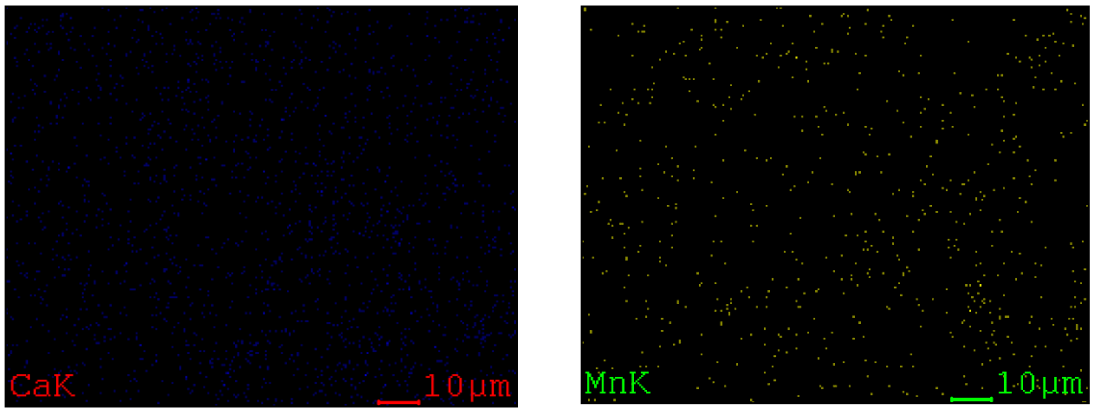

Figure 4.1: EDX Mapping of Ca and Mn Elements in CaO-MnO Adsorbent

From the Figure 4.1, it was observed that the distribution of Ca and Mn elements were uniform. The EDX mapping results further confirmed that sol-gel method not only can produced correct elements composition, but also produce uniform distribution of MnO on the surface of CaO.

4.1.3 X-ray Diffraction (XRD) Analysis

The XRD patterns for pure CaO and CaO-MnO adsorbent were shown in Figure 4.2. The XRD raw data was shown in Appendix D. Referring to the Joint Committee on Power Diffraction Standard (JCPDS), the main diffraction peak for CaO is around 2θ = 32.3º, 37.3º, 53.8º, 64.1º, 67.3ºand 79.7º (JCPDS File No. 00-037-1497). The main peaks for MnO were detected at 2θ = 28.8º, 30.1º, 37.3º, 41.0º, 42.9º, 46.1º, 56.7º, 59.3º and 72.2º (JCPDS File No. 00-024-0735). As for the peaks for $CaCO_3$ were at 2θ = 23.0º, 23.2º, 29.5º, 39.4º, 43.3º, 43.5º, 47.1º, 47.4º, 47.7º, 48.6º, 57.4º, 62.0 º and 65.0º (JCPDS File No. 00-047-1743).

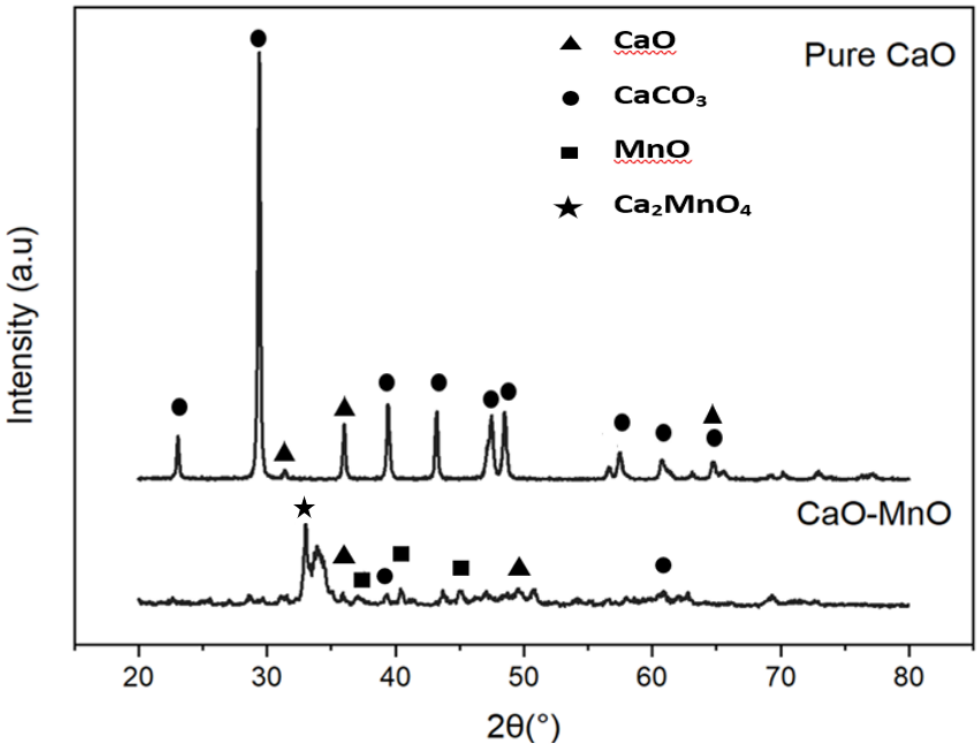

Figure 4.2: XRD Patterns of CaO and CaO-MnO Adsorbents

From the XRD pattern for pure CaO adsorbent, CaO peak was detected at 2θ = 32.3º, 37.3º and 64.1º. For the CaO-MnO adsorbent, peak for CaO is detected around 2θ = 32.3º, 37.3º, 53.8º, 64.1º, 67.3ºand 79.7º. The main peaks for MnO were detected at 2θ = 37.3º, 41.0º and 46.1º. From the XRD analysis, it showed that the CaO-MnO adsorbent consist of physical mixture of CaO and MnO. However, at peak 2θ = 34.0º in CaO-MnO XRD spectra, it was found the presence of calcium manganese (IV) oxide ($CaMnO_4$). The calcium manganese (IV) oxide was normally use as electrocatalyst for oxygen reduction reaction (ORR). Currently, there was no supporting paper on how the calcium manganese (IV) oxide can affects the CO_2 adsorption process.

Furthermore, it was observed that there was a lot of $CaCO_3$ peak especially in CaO XRD spectra. For CaO adsorbent, the peak of $CaCO_3$ were at 2θ = 23.2º, 29.5º, 39.4º 43.5º, 47.7º, 48.6º, 57.4º, 62.0 º and 65.0º. While the peak of $CaCO_3$ in CaO-MnO were at 2θ = 39.4º and 62.0°. This was because the $CaCO_3$ was formed after the calcination process in adsorbent synthesis steps, where the calcinated sample was cooled. Some pretreatment should be done to the carbonated sample before use in order to obtain more accurate results.

By assuming some condition of the crystalline such as shape factor, the crystalline size can be estimated by using the Scherrer's equation. The crystallite size which approximated by the Debye-Scherrer's equation is the mean size of the particular crystalline. Since the equation only yield the mean size of the crystallite, the 3 strongest peaks were used to calculate the crystallite size. Sample calculation for the crystallite size is shown in Appendix D and the calculation results were tabulated in Table 4.4 and Table 4.5.

Table 4.4: XRD Data of CaO Adsorbent

No.	**Peak No.**	**2θ (°)**	**2θ (rad)**	**FWHM (°)**	**FWHM (rad)**	**Mean Crystallite Size, τ (nm)**
1	2	29.3898	0.256474	0.2183	0.00381	39.2933
2	5	39.4165	0.343974	0.2169	0.003786	40.63359
3	10	48.4965	0.423212	0.2627	0.004585	34.64029
					Average Crystallite Size	38.18906

Table 4.5: XRD Data of CaO-MnO Adsorbent

No.	**Peak No.**	**2θ (°)**	**2θ (rad)**	**FWHM (°)**	**FWHM (rad)**	**Mean Crystallite Size, τ**
1	11	33.006	0.288032	0.3774	0.006587	22.92963
2	13	34.44	0.300546	0.3912	0.006828	22.20482
3	19	40.423	0.352757	0.3231	0.005639	27.36486
					Average Crystallite Size	24.16643

From the computed results in Table 4.4 and 4.5, it shown that the crystallite size of CaO-MnO adsorbent was smaller than CaO adsorbent. This results further confirmed the results found in SEM imaging. The presence of MnO not only reduced the crystallite size of the adsorbent, but also changes the crystal structure of the CaO adsorbent.

4.2 CO_2 Adsorption Study

In order to study the CO_2 adsorption performance of the synthesized calcium oxide-manganese oxide (CaO-MnO) adsorbent at different temperature, the carbonation reaction of the adsorbent was carried out in Thermal Gravimetric Analyser (TGA) at temperature of 463 °C, 500 °C and 590 °C. From the TGA, a graph of adsorbent weight changes with time can be obtained. The weight change of the adsorbent represents the weight of carbon dioxide (CO_2) adsorbed in the carbonation process to convert CaO to calcium carbonate ($CaCO_3$). The TGA results was analysed and tabulated in Appendix A. The TGA results were used to calculate the adsorption capacity of the adsorbent and further used to perform kinetic study on the CaO-MnO adsorbent in CO_2 capture.

4.2.1 CO_2 Adsorption Diffusion-limited and Reaction-limited Stages

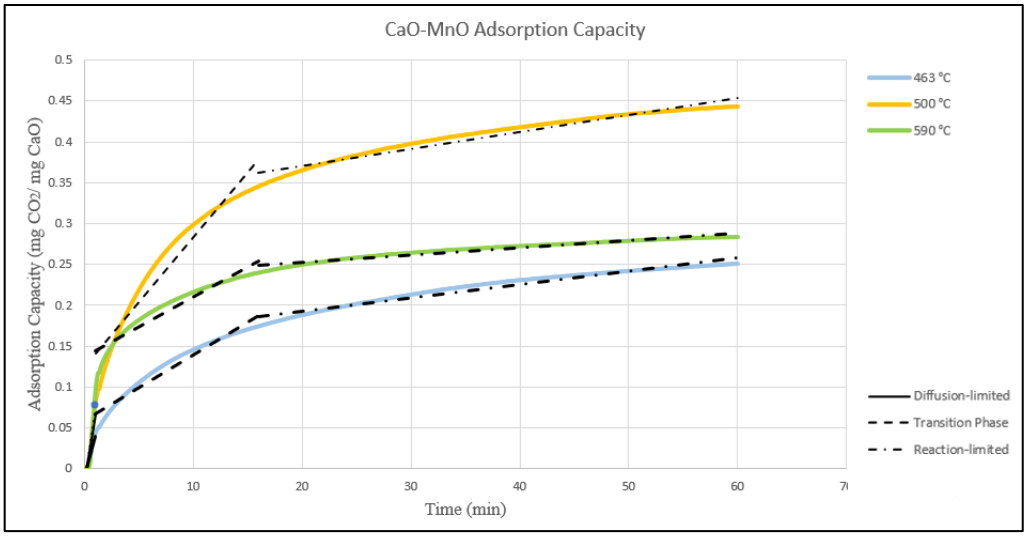

Figure 4.3: Adsorption Capacity of CaO-MnO Adsorbent at Different Temperature

From the gradient of CO_2 adsorption capacity in Figure 4.3, it can be seen that the initial adsorption rate increased rapidly at first minute as proven by the steep gradient of the graph. After a minute, the adsorption rate started to reduced. As time passed, the adsorption capacity will slowly approached a constant value which indicates zero CO_2 adsorption rate.

It was evident that the CO_2 capture performed at different rates at different stages. Firstly, the high CO_2 adsorption rate during carbonation reaction at first minute can be considered occurred at diffusion-limited stage. During diffusion-

limited stage, the carbonation reaction occurs on the CaO-MnO surface which consists of high amounts of free active site. At this stage, the adsorption rate is only limited by the diffusion or transportation rate of CO_2 onto the surface of the adsorbent.

Next, the reduction of CO_2 adsorption rate after the first minute suggested the transition phase of the carbonation reaction from diffusion-limited stage to reaction-limited stage. At this transition phase, due to the carbonation of CaO, more $CaCO_3$ formed on the surface of the adsorbent which occupy the active sites of the adsorbent. Therefore, the CO_2 adsorption rate started to reduced and resricted by the reduction of surface reaction.

Finally, the CO_2 adsorption rate was further decreased and eventually reached zero in reaction-limited stage. The reaction between the adsorbent and CO_2 was further limited by the increasing difficulty of CO_2 to diffuse through the carbonated layer to react with unreacted CaO-based adsorbent near the core (Nimmas et al., 2018). Hence, the carbonation reaction rate is limited as there is no more approachable unreacted CaO-based adsorbent. In this stage, the CO_2 adsorption capacity profile should conclude with a plateau. However, it was noticed that the CO_2 adsorption profile for all carbonation temperature had not reach constant value. This may because the 60 minutes duration was not enough for the adsorbents to react completely.

4.2.2 CO_2 Adsorption Rates

After studying the TGA results, the CO_2 adsorption rate of the adsorbent (CaO-MnO) was calculated based on the TGA data. The CO_2 adsorption rate shows the amount of CO_2 adsorbed and reacted with the adsorbent to form $CaCO_3$ at a unit of time. A sample calculation for CO_2 adsorption rate is shown in Appendix B and the calculated CO_2 adsorption rate at different stages were tabulated in Table 4.6.

Table 4.6: CO_2 Adsorption Rate of CaO-MnO Adsorbent at Different Temperatures and Stages

Carbonation Temperature (°C)	**CO_2 Adsorption Rate (mg CO_2/ mg CaO min)**		
	Diffusion-limited	**Transition Phase**	**Reaction-limited**
463	0.0423	0.0088	0.0017
500	0.0768	0.0179	0.0022
590	0.0873	0.0102	0.0010

Increase in carbonation temperature will helps in increasing the CO_2 adsorption rate of the CaO-based adsorbent. According to collision theory, the reactants need to collide with each other with sufficient energy for reaction to occur. Increase in reaction temperature provides more kinetic energy for the reactants which results increase in collision frequency between reactants. Thus, the sufficient energy and high collision frequency contribute to high effective collision between the reactants. Having more effective collision also means that the reactants are able to break and form bonds with ease in the reaction of forming $CaCO_3$. Therefore, high adsorption rate can be achieved at higher carbonation temperature.

Based on the calculated CO_2 adsorption rate in Table 4.6, the CO_2 adsorption rate was the highest at diffusion-limited stage where there was ample free surface of unreacted CaO. During transition phase, the adsorption rate reduced due to the increasing formation of $CaCO_3$ layer which hinder the CO_2 from reacting with remaining unreacted CaO. The adsorption rate in reaction-limited stage was the lowest among the three stages because the increase in the $CaCO_3$ layer thickness further hinder the diffusion of CO_2 from reaching the unreacted CaO core.

However, in transition stage and reaction-limited stage, it was observed that the CO_2 adsorption rate reduced at temperature of 590 °C. This may happen due to CaO carbonation reaction is physical adsorption where the reaction is reversible. Suppose, a gas phase and solid phase reactants interacting with each other. In this case, it is CO_2 gas with solid CaO-MnO adsorbent. The CO_2 gas molecules reacted and attached to the CaO-MnO adsorbent surface and release heat since it is exothermic reaction. When higher temperature was provided to the adsorbed CO_2, the CO_2 molecules obtained enough energy to detached from the CaO-MnO

adsorbent surface. Therefore, the rate of CO_2 adsorption decreases as some $CaCO_3$ reversed back to CaO by releasing CO_2.

Table 4.7: CO_2 Adsoprtion Rate of pure CaO

Adsorbent	**Carbonation Temperature (°C)**	**CO_2 Adsorption Capacity (mg CO_2/ mg CaO min)**	**Reference**
CaO-MnO	500	0.0074	*This project
Pure CaO	500	0.0059	Law, 2009

From the literature findings tabulated in Table 4.7, it was found that the addition of MnO into CaO adsorbent will helps in enhancing CO_2 capture rate. Referring to the literatures results, at carbonation temperature of 500 °C, the CO_2 adsorption rate of pure CaO adsorbent was 0.0059 mg CO_2/ mg CaO, while the CO_2 adsorption capacity of pure CaO-MnO adsorbent was 0.0074 mg CO_2/ mg CaO. According to the SEM results, CaO-MnO adsorbent also consist of smaller particle size compared to CaO. Therefore, CaO-MnO had increased surface area for more effective collsion in CO_2 adsorption process. Increase in effective collision frequency eventually increases the rate of CO_2 carbonation.

4.2.3 Adsorption Capacity

According to the TGA results, the CO_2 adsorption capacity for CaO-MnO adsorbent at different stages were calculated and tabulated in Table 4.8. The sample calculation for the CO_2 adsorption capacity was shown in Appendix B. The CO_2 adsorption capacity shows the amount of CO_2 captured by the adsorbent per a unit mass of CaO adsorbent used.

From the Figure 4.3, it can be observed that the CO_2 adsorption capacity of CaO-MnO adsorbent was the highest at carbonation temperature of 500 °C. The CO_2 adsorption capacity at carbonation temperature of 590 °C was lower because the CO_2 desorption may occur during the high temperature. The high energy produced by the high carbonation temperature and exothermic reaction heat allowed the adsorbed CO_2 molecules to detach from the $CaCO_3$. Hence, the CO_2 adsorption capacity was lower at carbonation temperature of 590 °C compared to carbonation temperature of

500 °C. The CO_2 adsorption capacity at carbonation temperature of 463 °C was lowest among the three carbonation temperature.

Table 4.8: CO_2 Adsorption Capacity of CaO-MnO Adsorbent at Different Temperatures and Stages

Carbonation Temperature (°C)	**CO_2 Adsorption Capacity (mg CO_2/ mg CaO)**			
	Diffusion-limited	**Transition Phase**	**Reaction-limited**	**Total**
463	0.0423	0.1316	0.0765	0.2504
500	0.0768	0.2679	0.0979	0.4426
590	0.0873	0.1525	0.0438	0.2836

Based on the results of CaO-MnO adsorption capacity, the transition phase had the highest amount of CO_2 captured for all three carbonation temperatures. This may due to the carbonation reaction only occur for short duration during the diffusion-limited stage. During the transition phase, there is more time for the adsorbent to capture and react with the CO_2 gas. Hence, higher amount of CO_2 was captured at transition phase instead of at diffusion-limited stage. As for reaction-limited stage, the CO_2 diffusion rate was hindered by the $CaCO_3$ layers formed. Thus, less amount of CO_2 was captured during the reaction-limited stage.

Furthermore, it was evident the highest CO_2 adsorption capacity was 0.4426 mg CO_2/ mg CaO at carbonation temperature of 500 °C. Theoretically, 1 mol of CaO react with 1 mol of CO_2 to form 1 mol of $CaCO_3$. In term of mass, at 100 % conversion, 56.0774 mg of CaO react with 44.01 mg of CO_2. Each milligram of CaO should be able to capture 0.7848 mg of CO_2. At carbonation temperature of 500 °C, the CO_2 adsorption capacity of 0.4426 mg CO_2/ mg CaO had not even reached 100 % conversion completely. This situation can also be seen in other two carbonation temperature (463 °C and 590 °C). The reaction time is insufficient for the adsorbent to react with CO_2 completely. From Figure 4.1, it can be observed that there no adsorption capacity profile concluded with a plateau. Therefore, a longer carbonation reaction time should be allowed for the adsorbent to be converted completely.

Table 4.9: CO_2 Adsoprtion Capacity of CaO-based Adsorbent

Adsorbent	Carbonation Temperature (°C)	CO_2 Adsorption Capacity (mg CO_2/ mg CaO)	Reference
Pure CaO	400	0.09	Law, 2018
	500	0.35	
	600	0.41	
Pure CaO	758	0.16	Li, 2009
CaO-MnO	463	0.2504	*This project
	500	0.4426	
	590	0.2836	

From the literature findings in Table 4.9, it was found that the addition of MnO into CaO adsorbent will help in enchancing capture capacity. According to the literatures, at carbonation temperature of 500 °C, the CO_2 adsorption capacity of pure CaO adsorbent was 0.35 mg CO_2/ mg CaO, while the CO_2 adsorption capacity of pure CaO-MnO adsorbent was 0.4426 mg CO_2/ mg CaO. This may due to the addition of MnO into CaO-based adsorbent increase the porosity of the CaO-based adsorbent. According to the SEM results, CaO-MnO adsorbent also consist of smaller particle size compared to CaO. Therefore, CaO-MnO had increased surface area. Increease in porosity and surface area on the adsorbent surface facilitate the diffusion of the CO_2 onto the CaO surface.

4.3 Kinetic Study

Kinetic analysis on CO_2 adsorption of CaO-based adsorbent is significant to the investigation on the adsorption process during carbonation reaction. In this experiment, different type of kinetic models compiled by Wei et al. (2017) was applied for different carbonation reaction regions. Firstly, zero-order (R1), first-order (A1), second-order (F2) and third-order (F3) reaction models were used for diffusion-limited region reaction. For transition phase and reaction-limited region, one-dimensional diffusion (D1), two-dimensional diffusion (D2), three-dimensional diffusion Jander equation (D3) and three-dimensional diffusion Ginstling-

Brounshtein (D4) were applied. Besides, another simpler version CaO carbonation kinetic model developed by Lee (2003) was also applied to study the adsorption process of the adsorbent.

4.3.1 CO_2 Adsorption Kinetic Models

In this kinetic analysis, the extent of conversion was calculated first and a graph was plotted based on the selected reaction model equations. The sample calculation for extent of conversion was included in Appendix B. From the graph plotted, the linear line least square method was used to determine the model fitting for respective reaction model and reaction stages. The results for diffusion-limited stage, transition phase and reaction-limited stage were shown in Table 4.10, Table 4.11 and Table 4.12 respectively.

Table 4.10: CO_2 Adsorption Model Fitting at Diffusion-limited Stage

Reaction Model	**Carbonation Temperature, T (°C)**	**Rate Constant, k (min^{-1})**	**R^2 of g(α) against t**	**Activation Energy, E_a (kJ/mol)**	**Pre-exponential factor, A (min^{-1})**	**R^2 of ln(k) against 1/T**
R1	463	0.1939	0.8831	20.7542	5.3324	0.8651
	500	0.1885	0.8573			
	590	0.3069	0.8099			
A1	463	0.2101	0.8786	23.6143	9.1349	0.8685
	500	0.2041	0.8505			
	590	0.3545	0.7904			
F2	463	0.2281	0.8736	26.8093	16.5453	0.8718
	500	0.2215	0.8430			
	590	0.4134	0.7682			
F3	**463**	**0.2484**	**0.8680**	**30.3153**	**31.5887**	**0.8742**
	500	**0.241**	**0.8347**			
	590	**0.4869**	**0.7433**			

Table 4.11: CO_2 Adsorption Model Fitting at Transition Phase

Reaction Model	Carbonation Temperature, T (°C)	Rate Constant, k (min^{-1})	R^2 of g(α) against t	Activation Energy, E_a (kJ/mol)	Pre-exponential factor, A (min^{-1})	R^2 of ln(k) against 1/T
D1	463	0.0304	0.9925	3.0322	0.05441	0.0970
	500	0.0386	0.9775			
	590	0.0342	0.9574			
D2	463	0.0215	0.9987	11.2023	0.1468	0.5718
	500	0.0294	0.9924			
	590	0.0295	0.9817			
D3	**463**	**0.0070**	**0.9991**	**21.6522**	**0.2658**	**0.8076**
	500	**0.0106**	**0.9992**			
	590	**0.0124**	**0.9976**			
D4	463	0.0054	0.9996	14.7898	0.0667	0.6738
	500	0.0077	0.9961			
	590	0.0081	0.9891			

Table 4.12: CO_2 Adsorption Model Fitting at Reaction-limited Stage

Reaction Model	Carbonation Temperature, T (°C)	Rate Constant, k (min^{-1})	R^2 of g(α) against t	Activation Energy, E_a (kJ/mol)	Pre-exponential factor, A (min^{-1})	R^2 of ln(k) against 1/T
D1	463	0.0114	0.9715	-27.4221	0.0001	0.9848
	500	0.0085	0.9655			
	590	0.0058	0.9545			
D2	463	0.0146	0.9975	-18.4538	0.0007	0.9933
	500	0.0122	0.9955			
	590	0.0093	0.9887			
D3	463	0.0127	0.9152	-3.0490	0.0078	0.7633
	500	0.0129	0.9335			
	590	0.0119	0.9282			

Table 4.12 (Continued)

	463	**0.0051**	**0.9949**			
D4	**500**	**0.0046**	**0.9972**	**-13.3598**	**0.0006**	**1.000**
	590	**0.0037**	**0.9938**			

Referring to the results obtained from least square method, model that had the highest R^2 value for g(α) against t and ln(k) against 1/T graphs was able to explain the kinetics of CO_2 adsorption process of the adsorbent. From Table 4.10, third-order (F3) reaction model is the best kinetic model to explain the CO_2 capture by the adsorbent at diffusion-limited stage. According to Table 4.11, three-dimensional diffusion Jander equation (D3) reaction model can be used to describe the adsorbent CO_2 adsorption in both transition phase and reaction-limited stage. Three-dimensional diffusion Ginstling-Brounshtein (D4) reaction model was more suitable to explain the CO_2 adsorption process of the adsorbent at reaction-limited stage. Three-dimensional diffusion Ginstling-Brounshtein (D4) reaction models most suitable for reaction-limited reaction of spherical model (Khawan and Flanagan, 2006).

The graphs of g(α) against t at carbonation temperature 463 °C, 500 °C and 590 °C were shown in Figure 4.4, Figure 4.5 and Figure 4.6 respectively. Best fit line was also applied for each reaction stages profile to show the least squared of the reaction model profile. For all the graphs in the figures, the left y-axis represents the third-order (F3) reaction model equation for diffusion-limited stage, and the right y-axis represent reaction model equation g(α) for transition phase and reaction-limited stage. From the gradient of each best fit line on the reaction model profile, the value of rate constant, k can be obtained.

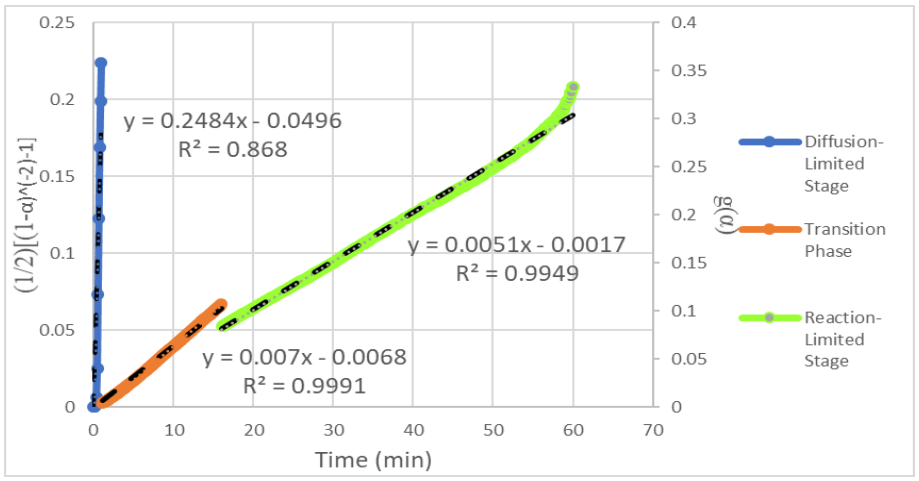

Figure 4.4: Kinetic Model and Linear Fitting at 463 °C

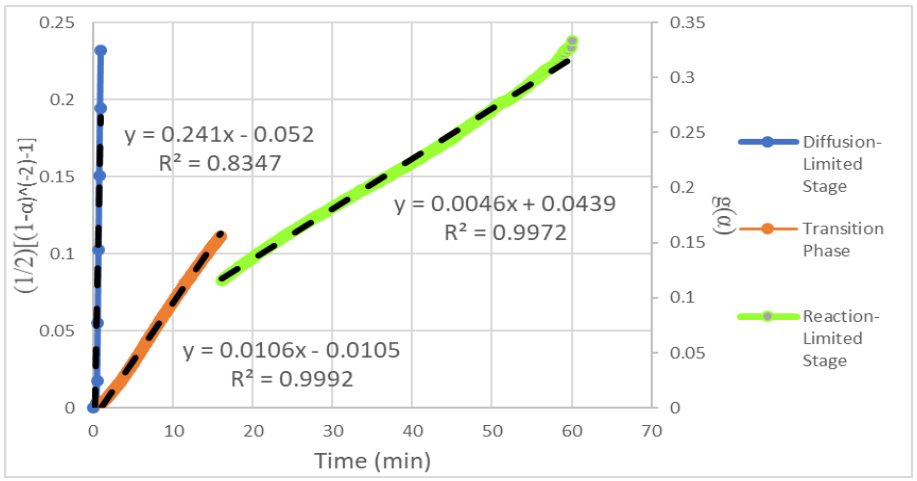

Figure 4.5: Kinetic Model and Linear Fitting at 500 °C

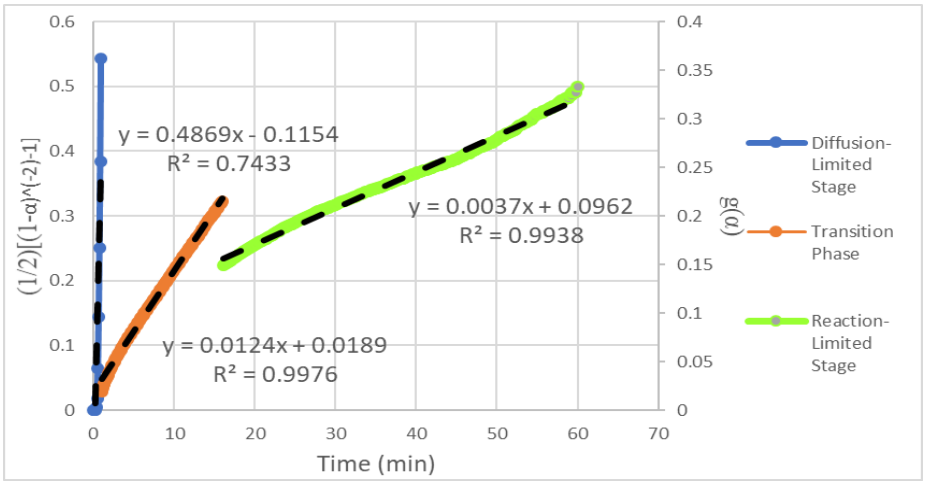

Figure 4.6: Kinetic Model and Linear Fitting at 590 °C

From the rate constant, k obtained from the graph, it was observed that the rate constant increases with increment of temperature at diffusion-limited stage and transition phase. The rate of CO_2 adsorption is proportional to the temperature (Wei et al., 2017). The rate of CO_2 adsorption will increase with temperature as long there was high vacancy of unreacted CaO surface. While in reaction-limited stage, the rate constant value decreases with increasing of temperature. This may due rapid formation of $CaCO_3$ layer caused high CO_2 adsorption rate at high temperature at diffusion-limited stage and transition phase. The $CaCO_3$ layer formed faster at high temperature and hence, the rate of CO_2 adsorption at reaction-limited stage reduced due to thicker $CaCO_3$ layer.

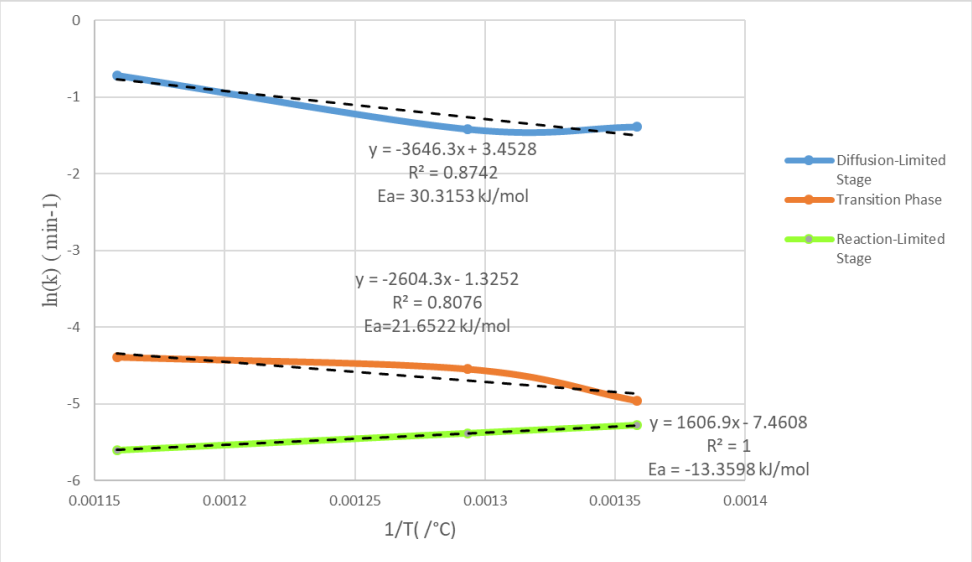

Figure 4.7: Arrhenius Plot of CaO at Different Stage

Table 4.13: Activation Energy at Each Stage of CaO Adsorbent for CO_2 Capture

Sample	**Reaction Model**	**Rate-Limiting Stage**	**Activation Energy, E_a (kJ/mol)**	**Reference**
CaO	Shrinking Core Model (SCM)	Diffusion-Limited Transition Phase Reaction-Limited	31.06 102.79 78.79	Vitiyaa, 2018

After obtaining the rate constant, k value, graph of ln(k) vs 1/T was plotted and shown in Figure 4.7. The gradient of the best fit line was multiplied with universal gas constant, R to obtain the activation energy. For comparison purpose, activation energy of pure CaO adsorbent was cited and tabulated in Table 4.13. Despite the reference using SCM as reaction model, the data was usable because the reaction model have similar principle with the integral reaction model used in this experiment. It was noticed that the activation energy at all rate-limiting stages for CaO-MnO adsorbent was lower when compared to the pure CaO adsorbent. The presence of MnO into CaO reduce the activation energy at all stage and eventually increase the CO_2 adsorption rate (Gunathilake, 2016). With the addition of MnO, the activation energy at transition phase was reduced significantly. The presence of MnO in the CaO adsorbent may help in facilitating the transportation of CO_2 molecules through the $CaCO_3$ layer to reach the CaO surface. However, it was noticed that the activation energy was negative at reaction-limited stage. The negative activation indicates the reduce in probability of molecule collision where the CO_2 molecule may move further away from reaction site due to high momentum.

From this kinetic model results, it can be observed that the increasing carbonation temperature will increase the CO_2 adsorption rate and CO_2 adsorption capacity. However, when the carbonation temperature was too high, desorption of CO_2 may occur. Addition of MnO into CaO adsorbent helps in reducing the activation energy significantly at transition phase.

4.3.2 CaO Carbonation Kinetic Models

For this kinetic model analysis, the CaO conversion was calculated first and a graph was plotted based on the selected reaction model equations. The sample calculation for CaO conversion was included in Appendix B. From the graph plotted, the linear line least square method was used to determine the model fitting for respective reaction model and reaction stages. The results for Lee (2003) CaO carbonation kinetic model was tabulated in Table 4.14.

Table 4.14: CO_2 Adsorption Model Fitting

Reaction Model	**Carbonation Temperature, T (°C)**	**Rate Constant, k (min^{-1})**	**R^2 of 1/X against 1/t**	**Activation Energy, E (kJ/mol)**	**Pre-exponential factor, A (min^{-1})**	**R^2 of ln(k) against 1/T**
Lee	463	0.0135	0.4560	-9.8097	-5.8527	0.7558
	500	0.0143	0.3846			
	590	0.0110	0.3780			

From the results shown in Table 4.14, it was observed that the kinetic model line did not fit well with the TGA results. The R^2 of 1/X against 1/t was only around 0.3780 to 0.4560. This showed that the kinetic model could not describe the CO_2 adsorption reaction of CaO-MnO adsorbent.

CHAPTER 5

CONCLUSIONS AND RECOMMENDATIONS

5.1 Conclusions

In this project sol-gel method can be used to synthesise CaO-based adsorbent with addition of MnO. From the SEM analysis, the CaO-MnO adsorbent had finer crystallite size and higher porosity than pure CaO adsorbent. Based from the EDX results, the elements weight fraction of the synthesised CaO-MnO adsorbent and CaO adsorbent were almost the same with the theoretical elements weight fraction. The distribution of Ca and Mn elements in the CaO-MnO adsorbent were also evenly distributed as shown in the EDX mapping. For CaO adsorbent, the XRD shows that there is presence of CaO and $CaCO_3$ in the adsorbent. The XRD results shows the presence of CaO, MnO and $CaCO_3$ in the CaO-MnO adsorbent. However, there was presence of mixed metal oxide which was calcium manganese oxide ($CaMnO_4$) in CaO-MnO adsorbent. XRD analysis also further proved that the CaO-MnO adsorbent had smaller crystallite size than pure CaO adsorbent.

From the CO_2 adsorption profile, it was shown the CO_2 adsorption process was controlled by three different regimes which were diffusion-limited stage, transition stage and reaction-limited stage. From the TGA results, CaO-MnO adsorbent had highest adsorption rate of 0.0873 mg CO_2/ mg CaO at diffusion-limited stage at carbonation temperature 590 °C. CaO-MnO adsorbent had high capacity during transition phase due to longer duration of the stage. Overall, based on the TGA analysis, CaO-MnO adsorbent had the highest total CO_2 adsorption capacity of 0.4426 mg CO_2/ mg CaO at the temperature of 500 °C. When compared to other literature results, CaO-MnO adsorbent had higher adsorption capacity and rate than pure CaO adsorbent.

In the kinetic study, kinetic model proposed by Wei et al. (2017) was selected due to the high suitability to describe the CO_2 adsorption reaction. Suitable reaction models were selected for respective rate-limiting stage. Compared with other literature results on pure CaO adsorbent activation energy, it was found that addition of MnO into CaO-based adsorbent can reduce the activation energy to initiate the CO_2 adsorption process.

5.2 Recommendations for Future Work

In the TGA analysis, it was observed that the CaO-based adsorbent could not achieved 100% conversion within 60 minutes, as shown in the CO_2 adsorption capacity profile. Longer carbonation time was recommended in order for the CaO-based adsorbent to react completely. There were many researches done on the CO_2 adsorption for various CaO adsorbent added transition metal oxide. It was suggested to perform kinetics study on the CO_2 desorption mechanism on the CaO-MnO adsorbent.

REFERENCES

Abunowara, M. and Elgarni, M. (2013). Carbon Dioxide Capture from Flue Gases by Solid Sorbents. *Energy Procedia*, 37, pp.16-24.

Blamey, J., Zhao, M., Manovic, V., Anthony, E., Dugwell, D. and Fennell, P. (2016). A shrinking core model for steam hydration of CaO-based sorbents cycled for CO2 capture. *Chemical Engineering Journal*, 291, pp.298-305.

Breault, R. (2006). A review of gas–solid dispersion and mass transfer coefficient correlations in circulating fluidized beds. *Powder Technology*, 163(1-2), pp.9-17.

Breault, R. (2006). A review of gas–solid dispersion and mass transfer coefficient correlations in circulating fluidized beds. *Powder Technology*, 163(1-2), pp.9-17.

Chemistry, I. (2018). *IUPAC Gold Book*. [online] Goldbook.iupac.org. Available at: http://goldbook.iupac.org/ [Accessed 26 Aug. 2018].

D'Alessandro, D., Smit, B. and Long, J. (2010). ChemInform Abstract: Carbon Dioxide Capture: Prospects for New Materials. *ChemInform*, 41(48), p.no-no.

Feng, B., Liu, W., Li, X. and An, H. (2006). Overcoming the Problem of Loss-in-Capacity of Calcium Oxide in CO2Capture. *Energy & Fuels*, 20(6), pp.2417-2420.

Florin, N. and Fennell, P. (2011). Synthetic CaO-based sorbent for CO2 capture. *Energy Procedia*, 4, pp.830-838.

Fogler, H. (2015). *Elements of chemical reaction engineering*. 5th ed. Pearson.

Gong, X., Wang, Z., Wang, Z., Cao, J. and Zhang, S. (2018). Roles of impurities on sintering structure and thermal strength of CaO-containing carbon pellet and the CaO sintering kinetic analysis. *Powder Technology*, 336, pp.92-101.

He, Q., Yu, G., Yan, S., Dumée, L., Zhang, Y., Strezov, V. and Zhao, S. (2018). Renewable CO 2 absorbent for carbon capture and biogas upgrading by membrane contactor. *Separation and Purification Technology*, 194, pp.207-215.

Ho, Y. (2006). Review of second-order models for adsorption systems. *Journal of Hazardous Materials*, 136(3), pp.681-689.

Huang, C., Chang, K., Yu, C., Chiang, P. and Wang, C. (2010). Development of high-temperature CO2 sorbents made of CaO-based mesoporous silica. *Chemical Engineering Journal*, 161(1-2), pp.129-135.

Jensen, M., Pettersson, L., Swang, O. and Olsbye, U. (2005). CO_2 Sorption on MgO and CaO Surfaces: A Comparative Quantum Chemical Cluster Study. *The Journal of Physical Chemistry B*, 109(35), pp.16774-16781.

Kazi, S., Aranda, A., Meyer, J. and Mastin, J., 2014. High performance CaO-based

sorbents for pre- and post- combustion CO2 capture at high temperature. *Energy Procedia*, 63, pp.2207-2215.

Lee, D. (2004). An apparent kinetic model for the carbonation of calcium oxide by carbon dioxide. *Chemical Engineering Journal*, 100(1-3), pp.71-77.

Lee, M., Yogi Goswami, D., Kothurkar, N. and Stefanakos, E. (2015). Development and evaluation of calcium oxide absorbent immobilized on fibrous ceramic fabrics for high temperature carbon dioxide capture. *Powder Technology*, 274, pp.313-318.

Lee, M., Yogi Goswami, D., Kothurkar, N. and Stefanakos, E. (2015). Development and evaluation of calcium oxide absorbent immobilized on fibrous ceramic fabrics for high temperature carbon dioxide capture. *Powder Technology*, 274, pp.313-318.

Li, L., King, D., Nie, Z. and Howard, C. (2009). Magnesia-Stabilized Calcium Oxide Absorbents with Improved Durability for High Temperature CO_2 Capture. *Industrial & Engineering Chemistry Research*, 48(23), pp.10604-10613.

Li, Y., Zhao, C., Chen, H., Duan, L. and Chen, X. (2010). Cyclic CO_2 capture behavior of KMnO4-doped CaO-based sorbent. *Fuel*, 89(3), pp.642-649.

Li, Z., Cai, N. and Huang, Y. (2006). Effect of Preparation Temperature on Cyclic CO_2 Capture and Multiple Carbonation−Calcination Cycles for a New Ca-Based CO_2 Sorbent. *Industrial & Engineering Chemistry Research*, 45(6), pp.1911-1917.

Liu, W., An, H., Qin, C., Yin, J., Wang, G., Feng, B. and Xu, M. (2012). Performance Enhancement of Calcium Oxide Sorbents for Cyclic CO_2 Capture—A Review. *Energy & Fuels*, 26(5), pp.2751-2767.

Liu, W., Feng, B., Wu, Y., Wang, G., Barry, J. and Diniz da Costa, J. (2010). Synthesis of Sintering-Resistant Sorbents for CO_2 Capture. *Environmental Science & Technology*, 44(8), pp.3093-3097.

Lu, H., Reddy, E. and Smirniotis, P. (2006). Calcium Oxide Based Sorbents for Capture of Carbon Dioxide at High Temperatures. *Industrial & Engineering Chemistry Research*, 45(11), pp.3944-3949.

Lua, L., Murphy, C. and Blanchard, V. (2017). *Second-Order Reactions*. [online] Chemistry LibreTexts. Available at: https://chem.libretexts.org/Textbook_Maps/Physical_and_Theoretical_Chemistry_Textbook_Maps/Supplemental_Modules_(Physical_and_Theoretical_Chemistry)/Kinetics/Reaction_Rates/Second-Order_Reactions [Accessed 2 Aug. 2018].

Luo, C., Zheng, Y., Ding, N. and Zheng, C. (2011). Enhanced cyclic stability of CO_2 adsorption capacity of CaO-based sorbents using La_2O_3 or $Ca_{12}Al_{14}O_{33}$ as additives. *Korean Journal of Chemical Engineering*, 28(4), pp.1042-1046.

Manovic, V. and Anthony, E. (2009). Long-Term Behavior of CaO-Based Pellets Supported by Calcium Aluminate Cements in a Long Series of CO_2 Capture Cycles. *Industrial & Engineering Chemistry Research*, 48(19), pp.8906-8912.

Marques, A. (2007). *Sol-gel process: an overview*. [online] Lehigh.edu. Available at: https://www.lehigh.edu/imi/teched/LecBasic/Marques_Sol_gel.pdf [Accessed 1 Aug. 2018].

Mohammadi, M., Lahijani, P. and Mohamed, A. (2014). Refractory dopant-incorporated CaO from waste eggshell as sustainable sorbent for CO_2 capture: Experimental and kinetic studies. *Chemical Engineering Journal*, 243, pp.455-464.

Nikulshina, V., Gálvez, M. and Steinfeld, A. (2007). Kinetic analysis of the carbonation reactions for the capture of CO_2 from air via the $Ca(OH)_2$–$CaCO_3$–CaO solar thermochemical cycle. *Chemical Engineering Journal*, 129(1-3), pp.75-8.

Nimmas, T., Jamrunroj, P., Wongsakulphasatch, S., Kiatkittipong, W., Laosiripojana,

N., Gong, J. and Assabumrungrat, S., 2018. Influence of CaO precursor on CO_2

capture performance and sorption-enhanced steam ethanol reforming. *International Journal of Hydrogen Energy*.

Roesch, A., Reddy, E. and Smirniotis, P. (2005). Parametric Study of Cs/CaO Sorbents with Respect to Simulated Flue Gas at High Temperatures. *Industrial & Engineering Chemistry Research*, 44(16), pp.6485-6490.

Safari, V., Arzpeyma, G., Rashchi, F. and Mostoufi, N. (2009). A shrinking particle—shrinking core model for leaching of a zinc ore containing silica. *International Journal of Mineral Processing*, 93(1), pp.79-83.

Salvador, C. (2003). Enhancement of CaO for CO_2 capture in an FBC environment. *Chemical Engineering Journal*.

Stewart, C. (2004). A study of methods of carbon dioxide capture and sequestration, the sustainability of a photosynthetic bioreactor approach. *Energy Conversion and Management*.

Tomaszewicz, G., Kotyczka-Morańska, M. and Plis, A., 2016. Studies on thecarbonation of Czatkowice limestone in Calcium Looping process. *Polish Journal ofChemical Technology*, 18(2), pp.53-58.

Wang, M., Lee, C. and Ryu, C. (2008). CO_2 sorption and desorption efficiency of Ca2SiO4. *International Journal of Hydrogen Energy*, 33(21), pp.6368-6372.

Wisaijorn, W., Praserthdam, P., Assabumrungrat, S. and Soisuwan, S. (2015). Modification of Green Calcium Oxide and Characteristics for Clean Energy Catalysts. *Energy Procedia*, 79, pp.685-690.

APPENDICES

APPENDIX A: TGA Raw Data

Table A1: TGA Raw Data

	Weight of CaO-MnO		
Time (min)	**463 °C**	**500 °C**	**590 °C**
0	18.505	12.319	18.347
0.1	18.505	12.318	18.347
0.2	18.505	12.318	18.347
0.3	18.507	12.318	18.347
0.4	18.516	12.326	18.355
0.5	18.549	12.355	18.382
0.6	18.625	12.428	18.467
0.7	18.694	12.509	18.59
0.8	18.751	12.583	18.722
0.9	18.785	12.643	18.853
1	18.812	12.69	18.975
1.1	18.834	12.728	19.079
1.2	18.855	12.76	19.146
1.3	18.873	12.789	19.192
1.4	18.874	12.789	19.193
1.5	18.892	12.816	19.23
1.6	18.908	12.841	19.258
1.7	18.924	12.865	19.283
1.8	18.939	12.888	19.306
1.9	18.954	12.909	19.326
2	18.968	12.93	19.345
2.1	18.981	12.95	19.363
2.2	18.994	12.969	19.379
2.3	19.007	12.989	19.395

Table A1 (Continued)

2.4	19.019	13.007	19.409
2.5	19.031	13.025	19.423
2.6	19.043	13.042	19.437
2.7	19.054	13.058	19.45
2.8	19.065	13.075	19.462
2.9	19.076	13.091	19.474
3	19.087	13.107	19.485
3.1	19.098	13.122	19.496
3.2	19.109	13.137	19.506
3.3	19.119	13.151	19.516
3.4	19.129	13.166	19.526
3.5	19.138	13.18	19.535
3.6	19.147	13.194	19.545
3.7	19.157	13.208	19.554
3.8	19.166	13.222	19.563
3.9	19.175	13.236	19.572
4	19.184	13.248	19.58
4.1	19.193	13.261	19.588
4.2	19.201	13.274	19.596
4.3	19.21	13.287	19.604
4.4	19.218	13.299	19.612
4.5	19.227	13.311	19.619
4.6	19.235	13.323	19.626
4.7	19.243	13.335	19.634
4.8	19.251	13.347	19.641
4.9	19.259	13.358	19.647
5	19.267	13.37	19.654
5.1	19.275	13.381	19.66
5.2	19.282	13.392	19.667
5.3	19.29	13.403	19.673
5.4	19.297	13.414	19.68

Table A1 (Continued)

5.5	19.304	13.424	19.686
5.6	19.311	13.434	19.693
5.7	19.318	13.444	19.699
5.8	19.326	13.454	19.705
5.9	19.333	13.464	19.711
6	19.34	13.474	19.717
6.1	19.347	13.483	19.722
6.2	19.354	13.492	19.727
6.3	19.36	13.501	19.733
6.4	19.367	13.511	19.738
6.5	19.373	13.52	19.744
6.6	19.379	13.528	19.749
6.7	19.386	13.537	19.755
6.8	19.392	13.545	19.76
6.9	19.398	13.553	19.765
7	19.404	13.561	19.77
7.1	19.41	13.57	19.775
7.2	19.416	13.578	19.78
7.3	19.422	13.586	19.785
7.4	19.429	13.593	19.789
7.5	19.434	13.601	19.793
7.6	19.44	13.608	19.798
7.7	19.446	13.616	19.803
7.8	19.451	13.623	19.808
7.9	19.457	13.63	19.813
8	19.462	13.637	19.818
8.1	19.468	13.644	19.823
8.2	19.473	13.651	19.827
8.3	19.479	13.658	19.831
8.4	19.484	13.665	19.836
8.5	19.489	13.671	19.84

Table A1 (Continued)

8.6	19.494	13.677	19.844
8.7	19.5	13.684	19.848
8.8	19.505	13.69	19.853
8.9	19.51	13.696	19.857
9	19.514	13.702	19.861
9.1	19.519	13.708	19.865
9.2	19.524	13.713	19.868
9.3	19.528	13.719	19.873
9.4	19.533	13.725	19.877
9.5	19.538	13.73	19.881
9.6	19.542	13.736	19.885
9.7	19.546	13.741	19.889
9.8	19.55	13.746	19.893
9.9	19.554	13.751	19.897
10	19.559	13.756	19.9
10.1	19.563	13.762	19.905
10.2	19.567	13.767	19.909
10.3	19.572	13.771	19.912
10.4	19.576	13.777	19.916
10.5	19.58	13.782	19.919
10.6	19.584	13.787	19.922
10.7	19.588	13.792	19.926
10.8	19.592	13.797	19.929
10.9	19.596	13.801	19.933
11	19.6	13.805	19.936
11.1	19.605	13.81	19.94
11.2	19.609	13.815	19.943
11.3	19.613	13.82	19.947
11.4	19.617	13.825	19.95
11.5	19.621	13.83	19.953
11.6	19.625	13.834	19.956

Table A1 (Continued)

11.7	19.628	13.838	19.959
11.8	19.632	13.842	19.962
11.9	19.636	13.846	19.965
12	19.639	13.85	19.968
12.1	19.643	13.854	19.971
12.2	19.646	13.858	19.974
12.3	19.65	13.862	19.977
12.4	19.654	13.866	19.98
12.5	19.657	13.87	19.983
12.6	19.661	13.874	19.986
12.7	19.665	13.878	19.989
12.8	19.668	13.882	19.992
12.9	19.672	13.885	19.994
13	19.675	13.889	19.996
13.1	19.679	13.892	19.999
13.2	19.683	13.896	20.002
13.3	19.687	13.9	20.005
13.4	19.69	13.903	20.008
13.5	19.693	13.907	20.011
13.6	19.697	13.911	20.014
13.7	19.7	13.914	20.017
13.8	19.703	13.917	20.02
13.9	19.706	13.92	20.023
14	19.709	13.923	20.026
14.1	19.712	13.926	20.029
14.2	19.715	13.929	20.031
14.3	19.718	13.933	20.034
14.4	19.721	13.937	20.036
14.5	19.725	13.94	20.038
14.6	19.727	13.944	20.04
14.7	19.73	13.947	20.042

Table A1 (Continued)

14.8	19.733	13.95	20.044
14.9	19.736	13.953	20.047
15	19.739	13.955	20.049
15.1	19.742	13.958	20.052
15.2	19.745	13.961	20.054
15.3	19.748	13.964	20.057
15.4	19.751	13.967	20.059
15.5	19.754	13.97	20.061
15.6	19.756	13.973	20.064
15.7	19.759	13.976	20.066
15.8	19.762	13.979	20.068
15.9	19.765	13.981	20.07
16	19.767	13.984	20.072
16.1	19.77	13.987	20.074
16.2	19.772	13.99	20.076
16.3	19.775	13.993	20.078
16.4	19.778	13.995	20.08
16.5	19.781	13.998	20.082
16.6	19.784	14	20.084
16.7	19.786	14.003	20.086
16.8	19.789	14.006	20.087
16.9	19.792	14.009	20.089
17	19.795	14.012	20.091
17.1	19.797	14.014	20.093
17.2	19.8	14.017	20.095
17.3	19.802	14.019	20.098
17.4	19.805	14.021	20.1
17.5	19.807	14.024	20.102
17.6	19.81	14.026	20.103
17.7	19.813	14.029	20.105
17.8	19.815	14.031	20.107

Table A1 (Continued)

17.9	19.817	14.033	20.109
18	19.82	14.035	20.111
18.1	19.822	14.038	20.113
18.2	19.824	14.04	20.115
18.3	19.827	14.043	20.116
18.4	19.83	14.046	20.118
18.5	19.832	14.048	20.12
18.6	19.835	14.05	20.122
18.7	19.837	14.052	20.123
18.8	19.84	14.054	20.124
18.9	19.842	14.056	20.126
19	19.844	14.058	20.127
19.1	19.846	14.061	20.129
19.2	19.848	14.063	20.131
19.3	19.85	14.065	20.132
19.4	19.853	14.067	20.133
19.5	19.855	14.069	20.135
19.6	19.858	14.071	20.136
19.7	19.86	14.073	20.138
19.8	19.862	14.075	20.14
19.9	19.865	14.078	20.141
20	19.867	14.08	20.143
20.1	19.869	14.082	20.145
20.2	19.871	14.084	20.146
20.3	19.873	14.086	20.148
20.4	19.875	14.089	20.149
20.5	19.877	14.091	20.15
20.6	19.879	14.093	20.152
20.7	19.881	14.095	20.153
20.8	19.884	14.097	20.154
20.9	19.886	14.099	20.155

Table A1 (Continued)

21	19.888	14.101	20.157
21.1	19.89	14.103	20.158
21.2	19.892	14.105	20.159
21.3	19.895	14.106	20.16
21.4	19.897	14.108	20.161
21.5	19.899	14.11	20.163
21.6	19.901	14.112	20.164
21.7	19.902	14.113	20.165
21.8	19.904	14.115	20.167
21.9	19.907	14.117	20.168
22	19.908	14.119	20.169
22.1	19.911	14.121	20.171
22.2	19.912	14.123	20.172
22.3	19.914	14.124	20.174
22.4	19.916	14.126	20.175
22.5	19.918	14.128	20.177
22.6	19.92	14.13	20.178
22.7	19.922	14.132	20.179
22.8	19.924	14.133	20.181
22.9	19.926	14.135	20.182
23	19.927	14.137	20.183
23.1	19.929	14.139	20.185
23.2	19.931	14.141	20.186
23.3	19.933	14.142	20.187
23.4	19.935	14.144	20.189
23.5	19.937	14.145	20.19
23.6	19.939	14.147	20.191
23.7	19.941	14.149	20.192
23.8	19.943	14.15	20.193
23.9	19.945	14.152	20.194
24	19.946	14.153	20.194

Table A1 (Continued)

24.1	19.948	14.155	20.196
24.2	19.95	14.156	20.197
24.3	19.951	14.158	20.198
24.4	19.953	14.159	20.199
24.5	19.955	14.161	20.2
24.6	19.957	14.163	20.201
24.7	19.959	14.164	20.202
24.8	19.961	14.166	20.203
24.9	19.963	14.167	20.204
25	19.965	14.168	20.205
25.1	19.967	14.17	20.206
25.2	19.969	14.171	20.208
25.3	19.97	14.173	20.209
25.4	19.972	14.174	20.209
25.5	19.974	14.175	20.21
25.6	19.976	14.177	20.211
25.7	19.977	14.179	20.212
25.8	19.979	14.18	20.213
25.9	19.981	14.182	20.214
26	19.982	14.183	20.215
26.1	19.983	14.185	20.216
26.2	19.985	14.187	20.217
26.3	19.986	14.188	20.218
26.4	19.987	14.189	20.219
26.5	19.989	14.191	20.22
26.6	19.99	14.192	20.22
26.7	19.993	14.194	20.221
26.8	19.994	14.195	20.222
26.9	19.996	14.197	20.223
27	19.998	14.198	20.224
27.1	20	14.2	20.225

Table A1 (Continued)

27.2	20.002	14.201	20.226
27.3	20.004	14.203	20.227
27.4	20.005	14.204	20.228
27.5	20.007	14.206	20.229
27.6	20.009	14.207	20.23
27.7	20.01	14.209	20.231
27.8	20.012	14.21	20.232
27.9	20.013	14.211	20.232
28	20.015	14.212	20.233
28.1	20.017	14.213	20.234
28.2	20.018	14.214	20.235
28.3	20.02	14.215	20.236
28.4	20.022	14.216	20.236
28.5	20.024	14.217	20.237
28.6	20.025	14.219	20.237
28.7	20.027	14.22	20.237
28.8	20.029	14.221	20.238
28.9	20.03	14.222	20.239
29	20.032	14.223	20.239
29.1	20.033	14.224	20.24
29.2	20.035	14.225	20.241
29.3	20.037	14.227	20.242
29.4	20.038	14.228	20.243
29.5	20.04	14.23	20.244
29.6	20.041	14.231	20.244
29.7	20.043	14.233	20.245
29.8	20.044	14.234	20.246
29.9	20.046	14.236	20.246
30	20.047	14.237	20.247
30.1	20.048	14.238	20.248
30.2	20.05	14.239	20.249

Table A1 (Continued)

30.3	20.052	14.24	20.25
30.4	20.054	14.241	20.251
30.5	20.055	14.242	20.252
30.6	20.057	14.243	20.252
30.7	20.058	14.244	20.253
30.8	20.06	14.245	20.254
30.9	20.062	14.247	20.254
31	20.063	14.248	20.254
31.1	20.065	14.249	20.255
31.2	20.067	14.251	20.256
31.3	20.069	14.252	20.256
31.4	20.07	14.253	20.257
31.5	20.072	14.254	20.258
31.6	20.073	14.255	20.258
31.7	20.074	14.256	20.259
31.8	20.075	14.257	20.26
31.9	20.077	14.258	20.26
32	20.078	14.259	20.261
32.1	20.08	14.26	20.262
32.2	20.082	14.261	20.262
32.3	20.083	14.262	20.263
32.4	20.085	14.263	20.264
32.5	20.087	14.265	20.264
32.6	20.088	14.266	20.265
32.7	20.09	14.267	20.266
32.8	20.091	14.268	20.267
32.9	20.092	14.269	20.268
33	20.093	14.27	20.268
33.1	20.094	14.271	20.269
33.2	20.096	14.272	20.27
33.3	20.098	14.273	20.271

Table A1 (Continued)

33.4	20.099	14.275	20.271
33.5	20.101	14.276	20.272
33.6	20.102	14.277	20.273
33.7	20.103	14.278	20.274
33.8	20.104	14.278	20.274
33.9	20.105	14.279	20.274
34	20.106	14.28	20.275
34.1	20.108	14.281	20.275
34.2	20.109	14.282	20.276
34.3	20.11	14.283	20.276
34.4	20.111	14.284	20.277
34.5	20.113	14.285	20.277
34.6	20.114	14.286	20.278
34.7	20.116	14.286	20.278
34.8	20.117	14.287	20.279
34.9	20.119	14.289	20.279
35	20.12	14.29	20.28
35.1	20.122	14.291	20.28
35.2	20.123	14.292	20.281
35.3	20.124	14.293	20.281
35.4	20.125	14.293	20.282
35.5	20.126	14.294	20.282
35.6	20.127	14.295	20.283
35.7	20.128	14.295	20.284
35.8	20.129	14.296	20.284
35.9	20.131	14.298	20.285
36	20.132	14.299	20.286
36.1	20.133	14.3	20.286
36.2	20.134	14.302	20.287
36.3	20.135	14.303	20.287
36.4	20.137	14.303	20.288

Table A1 (Continued)

36.5	20.138	14.304	20.288
36.6	20.139	14.305	20.289
36.7	20.141	14.306	20.289
36.8	20.142	14.306	20.29
36.9	20.143	14.307	20.291
37	20.144	14.308	20.291
37.1	20.145	14.309	20.292
37.2	20.146	14.309	20.293
37.3	20.147	14.31	20.293
37.4	20.148	14.311	20.294
37.5	20.15	14.312	20.294
37.6	20.151	14.313	20.295
37.7	20.152	14.314	20.296
37.8	20.153	14.315	20.296
37.9	20.153	14.316	20.297
38	20.154	14.317	20.298
38.1	20.155	14.318	20.298
38.2	20.157	14.319	20.298
38.3	20.158	14.32	20.298
38.4	20.159	14.321	20.298
38.5	20.16	14.322	20.299
38.6	20.162	14.323	20.299
38.7	20.163	14.323	20.3
38.8	20.165	14.324	20.301
38.9	20.166	14.325	20.302
39	20.167	14.325	20.302
39.1	20.167	14.326	20.303
39.2	20.168	14.327	20.303
39.3	20.169	14.328	20.304
39.4	20.17	14.329	20.304
39.5	20.171	14.33	20.305

Table A1 (Continued)

39.6	20.172	14.33	20.305
39.7	20.173	14.331	20.305
39.8	20.175	14.332	20.306
39.9	20.176	14.333	20.306
40	20.176	14.334	20.307
40.1	20.177	14.335	20.308
40.2	20.178	14.336	20.308
40.3	20.179	14.337	20.309
40.4	20.179	14.338	20.309
40.5	20.18	14.339	20.309
40.6	20.181	14.34	20.31
40.7	20.182	14.34	20.31
40.8	20.183	14.341	20.31
40.9	20.184	14.341	20.311
41	20.185	14.342	20.311
41.1	20.187	14.343	20.312
41.2	20.188	14.344	20.312
41.3	20.189	14.345	20.312
41.4	20.19	14.346	20.313
41.5	20.19	14.347	20.313
41.6	20.191	14.348	20.313
41.7	20.191	14.349	20.314
41.8	20.192	14.35	20.315
41.9	20.193	14.351	20.315
42	20.194	14.351	20.316
42.1	20.194	14.352	20.316
42.2	20.196	14.353	20.317
42.3	20.197	14.353	20.317
42.4	20.198	14.354	20.318
42.5	20.199	14.355	20.318
42.6	20.2	14.356	20.319

Table A1 (Continued)

42.7	20.2	14.357	20.319
42.8	20.201	14.358	20.319
42.9	20.202	14.358	20.319
43	20.203	14.359	20.319
43.1	20.203	14.36	20.32
43.2	20.204	14.361	20.321
43.3	20.205	14.362	20.321
43.4	20.205	14.362	20.321
43.5	20.206	14.363	20.322
43.6	20.207	14.364	20.322
43.7	20.208	14.365	20.323
43.8	20.209	14.365	20.323
43.9	20.21	14.367	20.324
44	20.211	14.367	20.325
44.1	20.211	14.368	20.325
44.2	20.212	14.369	20.325
44.3	20.213	14.369	20.325
44.4	20.214	14.37	20.325
44.5	20.215	14.37	20.326
44.6	20.216	14.371	20.326
44.7	20.217	14.371	20.327
44.8	20.218	14.372	20.328
44.9	20.218	14.373	20.328
45	20.219	14.374	20.328
45.1	20.22	14.375	20.329
45.2	20.221	14.376	20.329
45.3	20.222	14.377	20.33
45.4	20.223	14.377	20.33
45.5	20.223	14.378	20.331
45.6	20.224	14.379	20.331
45.7	20.225	14.38	20.332

Table A1 (Continued)

45.8	20.226	14.382	20.333
45.9	20.226	14.383	20.333
46	20.227	14.384	20.334
46.1	20.228	14.384	20.335
46.2	20.228	14.385	20.335
46.3	20.228	14.386	20.335
46.4	20.229	14.386	20.335
46.5	20.23	14.387	20.336
46.6	20.231	14.388	20.336
46.7	20.232	14.389	20.337
46.8	20.233	14.389	20.338
46.9	20.234	14.39	20.339
47	20.235	14.391	20.339
47.1	20.236	14.392	20.339
47.2	20.236	14.392	20.339
47.3	20.237	14.393	20.34
47.4	20.237	14.394	20.34
47.5	20.238	14.395	20.341
47.6	20.239	14.395	20.342
47.7	20.24	14.396	20.343
47.8	20.24	14.396	20.343
47.9	20.241	14.397	20.344
48	20.242	14.397	20.344
48.1	20.243	14.398	20.344
48.2	20.243	14.399	20.344
48.3	20.244	14.4	20.345
48.4	20.245	14.401	20.345
48.5	20.245	14.402	20.345
48.6	20.246	14.402	20.346
48.7	20.247	14.403	20.346
48.8	20.247	14.404	20.346

Table A1 (Continued)

48.9	20.248	14.404	20.347
49	20.249	14.405	20.347
49.1	20.251	14.405	20.348
49.2	20.252	14.406	20.348
49.3	20.252	14.407	20.349
49.4	20.253	14.407	20.349
49.5	20.254	14.408	20.35
49.6	20.254	14.408	20.35
49.7	20.255	14.409	20.351
49.8	20.255	14.409	20.352
49.9	20.256	14.41	20.352
50	20.257	14.411	20.352
50.1	20.258	14.412	20.353
50.2	20.258	14.413	20.354
50.3	20.259	14.414	20.355
50.4	20.26	14.414	20.355
50.5	20.26	14.415	20.356
50.6	20.261	14.415	20.356
50.7	20.262	14.416	20.356
50.8	20.263	14.416	20.356
50.9	20.263	14.417	20.357
51	20.264	14.418	20.358
51.1	20.264	14.418	20.358
51.2	20.265	14.419	20.359
51.3	20.266	14.419	20.359
51.4	20.267	14.42	20.359
51.5	20.268	14.42	20.36
51.6	20.268	14.42	20.36
51.7	20.269	14.42	20.36
51.8	20.269	14.42	20.361
51.9	20.27	14.421	20.361

Table A1 (Continued)

52	20.271	14.421	20.362
52.1	20.271	14.422	20.362
52.2	20.272	14.422	20.362
52.3	20.272	14.423	20.363
52.4	20.273	14.423	20.363
52.5	20.274	14.424	20.364
52.6	20.274	14.425	20.365
52.7	20.275	14.425	20.366
52.8	20.275	14.426	20.366
52.9	20.276	14.426	20.366
53	20.277	14.427	20.367
53.1	20.278	14.428	20.367
53.2	20.278	14.428	20.367
53.3	20.279	14.429	20.368
53.4	20.28	14.429	20.369
53.5	20.28	14.43	20.369
53.6	20.281	14.43	20.369
53.7	20.282	14.431	20.369
53.8	20.283	14.431	20.37
53.9	20.283	14.432	20.37
54	20.284	14.432	20.37
54.1	20.284	14.433	20.37
54.2	20.285	14.433	20.371
54.3	20.285	14.434	20.371
54.4	20.286	14.434	20.372
54.5	20.287	14.435	20.373
54.6	20.287	14.436	20.373
54.7	20.288	14.436	20.374
54.8	20.289	14.436	20.374
54.9	20.289	14.437	20.375
55	20.29	14.438	20.375

Table A1 (Continued)

55.1	20.291	14.439	20.375
55.2	20.292	14.439	20.375
55.3	20.292	14.439	20.375
55.4	20.293	14.44	20.376
55.5	20.294	14.44	20.376
55.6	20.294	14.441	20.376
55.7	20.295	14.441	20.377
55.8	20.296	14.441	20.377
55.9	20.297	14.442	20.377
56	20.298	14.442	20.378
56.1	20.298	14.443	20.378
56.2	20.299	14.443	20.378
56.3	20.299	14.444	20.378
56.4	20.3	14.444	20.379
56.5	20.301	14.445	20.379
56.6	20.301	14.445	20.379
56.7	20.302	14.446	20.379
56.8	20.303	14.446	20.379
56.9	20.303	14.446	20.38
57	20.304	14.446	20.38
57.1	20.304	14.446	20.38
57.2	20.305	14.447	20.38
57.3	20.305	14.447	20.38
57.4	20.306	14.448	20.381
57.5	20.306	14.448	20.381
57.6	20.307	14.448	20.381
57.7	20.307	14.448	20.382
57.8	20.308	14.449	20.382
57.9	20.309	14.449	20.383
58	20.309	14.45	20.383
58.1	20.31	14.45	20.383

Table A1 (Continued)

58.2	20.311	14.451	20.383
58.3	20.311	14.451	20.383
58.4	20.312	14.452	20.384
58.5	20.312	14.452	20.384
58.6	20.313	14.452	20.384
58.7	20.313	14.453	20.384
58.8	20.314	14.453	20.384
58.9	20.315	14.454	20.384
59	20.316	14.454	20.385
59.1	20.317	14.455	20.385
59.2	20.318	14.455	20.385
59.3	20.318	14.455	20.386
59.4	20.319	14.455	20.386
59.5	20.319	14.455	20.386
59.6	20.32	14.456	20.386
59.7	20.321	14.456	20.386
59.8	20.321	14.456	20.386
59.9	20.322	14.456	20.387
60	20.322	14.457	20.387

APPENDIX B: Sample Calculation for CO2 Adsorption and Kinetic Study

From the TGA raw data for CaO-MnO adsorbent at 500 °C are as shown below,

m_o = 12.319 mg

m_t = 12.690 mg

t = 1 min

The CO_2 adsorption capacity can be calculated with Eq. 3.2.

$$CO_2\ adsorption\ capacity = \frac{m_t - m_o}{m_o \times x_{CaO}}$$

$$x_{CaO} = \frac{0.5\ mol \times 56.0774\ g/mol}{0.5\ mol \times 56.0074\ g/mol + 0.5\ mol\ \times 86.9368\ g/mol}$$
$$= 0.3921$$

$$CO_2\ adsorption\ capacity = \frac{12.690\ mg - 12.319}{12.319 \times 0.3921}$$
$$CO_2\ adsorption\ capacity = 0.0768\ \text{mg}\ CO_2/\ mg\ CaO$$

The CO_2 adsorption rate can be calculated with Eq. 3.3.

$$CO_2\ adsorption\ rate = \frac{m_t - m_o}{m_o \times x_{CaO} \times t}$$
$$CO_2\ adsorption\ rate = \frac{12.690\ mg - 12.319}{12.319 \times 0.3921 \times 1\ \text{min}}$$
$$CO_2\ adsorption\ rate = 0.0768\ mg\ CO_2\ /\ mg\ CaO\ min$$

To calculate the extend of conversion for kinetic model. Eq. 2.2 is used.

$$\alpha = \frac{m_o - m_t}{m_o - m_f}$$
$$\alpha = \frac{12.319 - 12.690}{12.319 - 14.457}$$
$$\alpha = 0.1735$$

APPENDIX C: EDX Sample Calculation

Theoretical mass fraction of pure CaO adsorbent

It was assumed there is presence of $CaCO_3$ formed during cooling after synthesising process.

Mass of CaO and $CaCO_3$ = $2\ mol \times 40.078 \frac{g}{mol} + 1\ mol \times 12.0107 \frac{g}{mol} + 4\ mol \times 15.999\ g/mol$

Mass of CaO and $CaCO_3$ = 156.1627 g

$$Mass\ fraction\ of\ Ca = \frac{2\ mol\ \times 40.078}{156.1627\ g} = 0.5133$$

$$Mass\ fraction\ of\ O = \frac{4\ mol\ \times 15.999}{156.1627\ g} = 0.4098$$

$$Mass\ fraction\ of\ C = \frac{1\ mol\ \times 12.0107}{156.1627\ g} = 0.0769$$

Theoretical mass fraction of CaO-MnO adsorbent

It was assumed there is presence of $CaCO_3$ formed during cooling after synthesising process.

Mass of CaO-MnO and $CaCO_3$ = $1\ mol \times 40.078 \frac{g}{mol} + 0.5\ mol \times 12.0107 \frac{g}{mol} + 2.5\ mol \times 15.999 \frac{g}{mol} + 0.5 \times 54.93804\ g/mol$

Mass of CaO-MnO and $CaCO_3$ = 113.5499 g

$$Mass\ fraction\ of\ Ca = \frac{1\ mol\ \times 40.078}{113.5499\ g} = 0.3530$$

$$Mass\ fraction\ of\ Mn = \frac{0.5\ mol\ \times 54.93804}{113.5499\ g} = 0.2419$$

$$Mass\ fraction\ of\ O = \frac{2.5\ mol\ \times 15.999}{113.5499\ g} = 0.3522$$

$$Mass\ fraction\ of\ C = \frac{0.5\ mol\ \times 12.0107}{113.5499\ g} = 0.3530$$

APPENDIX D: XRD Calculation and Raw Data

The mean crystallite size can be calculation with Eq. 3.1

$$\tau = \frac{0.94\lambda}{FWHM \times Cos\,\theta}$$

From the CaO XRD data, one of the three highest peaks was at peak no. 2, where the 2θ=29.3898° and FWHM = 0.2183°

2θ=29.3898° = 0.2565 rad
FWHM = 0.2183° = 0.0038 rad

$$\tau = \frac{0.94(0.154056)}{0.0038 \times Cos\,0.2565}$$
$$\tau = 39.2933\ nm$$

*** Basic Data Process ***

Group : LeeZhiHua
Data : CaOLow

Strongest 3 peaks

no.	peak no.	2Theta (deg)	d (A)	I/I1	FWHM (deg)	Intensity (Counts)	Integrated Int (Counts)
1	2	29.3898	3.03660	100	0.21830	2063	25392
2	5	39.4165	2.28419	18	0.21690	380	4393
3	10	48.4965	1.87562	17	0.26270	344	5505

Peak Data List

peak no.	2Theta (deg)	d (A)	I/I1	FWHM (deg)	Intensity (Counts)	Integrated Int (Counts)
1	23.0573	3.85424	9	0.21810	186	2479
2	29.3898	3.03660	100	0.21830	2063	25392
3	29.7400	3.00164	4	0.14180	88	1733
4	36.0018	2.49262	12	0.23900	247	3458
5	39.4165	2.28419	18	0.21690	380	4393
6	39.6400	2.27183	3	0.12300	64	719
7	43.1884	2.09303	17	0.21210	341	4323
8	47.0800	1.92870	6	0.22540	116	1586
9	47.4011	1.91638	15	0.38220	318	5464
10	48.4965	1.87562	17	0.26270	344	5505
11	57.4440	1.60292	6	0.30400	134	2837
12	60.7472	1.52343	5	0.34550	97	2569
13	64.7185	1.43920	4	0.29430	91	1975

```
        ***  Basic Data Process  ***

# Data Infomation
          Group               : LeeZhiHua
          Data                : CaOLow
          Sample Nmae         : CaOLow
          Comment             :
          Date & Time         : 02-12-19 14:58:55

# Measurement Condition
    X-ray tube
          target              : Cu
          voltage             : 40.0 (kV)
          current             : 30.0 (mA)
    Slits
          Auto Slit           : not Used
          divergence slit     :   1.00000 (deg)
          scatter slit        :   1.00000 (deg)
          receiving slit      :   0.30000(mm)
    Scanning
          drive axis          : Theta-2Theta
          scan range          :   20.0000 - 80.0000 (deg)
          scan mode           : Continuous Scan
          scan speed          :    1.2000 (deg/min)
          sampling pitch      :    0.0200 (deg)
          preset time         :    1.00 (sec)

# Data Process Condition
    Smoothing                 [ AUTO ]
          smoothing points    : 13
    B.G.Subtruction           [ AUTO ]
          sampling points     : 13
          repeat times        : 30
    Ka1-a2 Separate           [ MANUAL ]
          Ka1 a2 ratio        : 50 (%)
    Peak Search               [ AUTO ]
          differential points : 11
          FWHM threhold       : 0.050 (deg)
          intensity threhold  : 30 (par mil)
          FWHM ratio  (n-1)/n : 2
    System error Correction   [ NO ]
    Precise peak Correction   [ NO ]
```

< Group: LeeZhiHua Data: CaOLow >

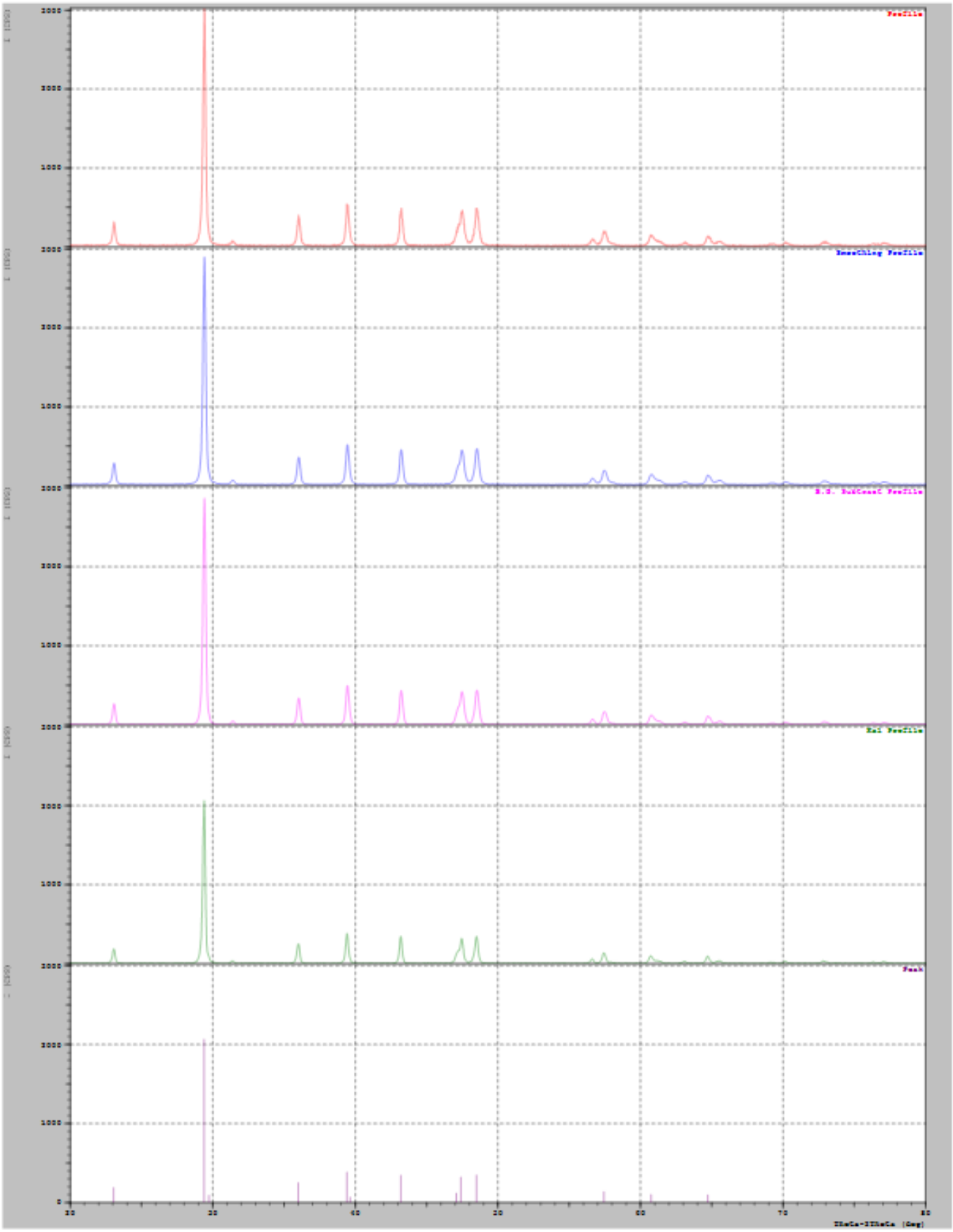

*** Basic Data Process ***

Group : LeeZhiHua
Data : CaOmnOLow

Strongest 3 peaks

no.	peak no.	2Theta (deg)	d (A)	I/I1	FWHM (deg)	Intensity (Counts)	Integrated Int (Counts)
1	11	33.0060	2.71170	100	0.37740	362	6024
2	12	33.9200	2.64069	70	0.00000	252	0
3	13	34.4400	2.60200	48	0.39120	173	3547

Peak Data List

peak no.	2Theta (deg)	d (A)	I/I1	FWHM (deg)	Intensity (Counts)	Integrated Int (Counts)
1	22.6633	3.92035	6	0.27330	22	219
2	24.8400	3.58152	3	0.26000	11	101
3	25.3943	3.50459	5	0.54860	18	247
4	27.0733	3.29093	5	0.25330	19	131
5	28.6321	3.11521	10	0.39570	37	394
6	29.2800	3.04774	4	0.34660	13	138
7	29.6460	3.01094	7	0.31600	26	192
8	31.0400	2.87882	8	0.32000	30	358
9	31.5200	2.83607	9	0.16000	31	195
10	32.2800	2.77101	5	0.30000	18	196
11	33.0060	2.71170	100	0.37740	362	6024
12	33.9200	2.64069	70	0.00000	252	0
13	34.4400	2.60200	48	0.39120	173	3547
14	35.0000	2.56164	14	0.43640	49	709
15	35.9071	2.49898	10	0.30570	36	247
16	36.1600	2.48208	3	0.26000	11	86
17	37.1000	2.42132	9	0.60000	31	520
18	39.2730	2.29221	12	0.35400	43	437
19	40.4230	2.22961	18	0.32310	66	583
20	41.0400	2.19750	4	0.16000	16	72
21	41.3450	2.18199	6	0.35000	22	207
22	43.6818	2.07053	13	0.32360	48	479
23	45.0428	2.01108	13	0.40570	48	512
24	46.2700	1.96056	3	0.40660	11	113
25	47.0420	1.93016	9	0.44400	32	281
26	47.3600	1.91794	4	0.28800	13	119
27	48.3600	1.88059	6	0.36000	20	180
28	48.6800	1.86898	7	0.24000	25	177
29	49.5200	1.83922	15	0.49600	55	612
30	49.8400	1.82816	9	0.29340	33	264
31	50.7389	1.79786	17	0.40220	60	704
32	53.7600	1.70374	4	0.19200	13	83
33	54.0400	1.69557	6	0.36000	21	139
34	54.3200	1.68749	5	0.30220	19	153
35	55.1306	1.66458	4	0.32530	14	135
36	56.4820	1.62792	6	0.36400	23	289
37	57.9520	1.59007	9	0.30400	32	257
38	58.5228	1.57592	4	0.48570	13	162
39	59.2566	1.55814	3	0.27330	11	80
40	59.7100	1.54739	5	0.30000	19	171
41	60.4400	1.53043	11	0.25600	41	311
42	60.8400	1.52133	13	0.44440	48	510
43	61.9920	1.49579	9	0.32000	34	367
44	62.7180	1.48021	12	0.31600	44	386
45	63.0800	1.47259	3	0.16000	11	54
46	66.1946	1.41064	4	0.19730	13	108
47	68.8400	1.36275	5	0.44000	18	253
48	69.2800	1.35516	10	0.53340	38	517
49	70.7400	1.33073	4	0.28000	13	107

peak no.	2Theta (deg)	d (A)	I/I1	FWHM (deg)	Intensity (Counts)	Integrated Int (Counts)
50	71.0600	1.32552	4	0.28000	13	88
51	71.4653	1.31900	4	0.24270	16	100
52	71.8500	1.31288	4	0.22000	13	79
53	72.5200	1.30239	4	0.32000	13	108
54	72.8800	1.29684	3	0.26000	11	89

```
         ***  Basic Data Process  ***

# Data Infomation
          Group                : LeeZhiHua
          Data                 : CaOmnOLow
          Sample Nmae          : CaOmnOLow
          Comment              :
          Date & Time          : 02-12-19 14:05:25

# Measurement Condition
    X-ray tube
          target               : Cu
          voltage              : 40.0 (kV)
          current              : 30.0 (mA)
    Slits
          Auto Slit            : not Used
          divergence slit      :   1.00000 (deg)
          scatter slit         :   1.00000 (deg)
          receiving slit       :   0.30000(mm)
    Scanning
          drive axis           : Theta-2Theta
          scan range           :   20.0000 - 80.0000 (deg)
          scan mode            : Continuous Scan
          scan speed           :    1.2000 (deg/min)
          sampling pitch       :    0.0400 (deg)
          preset time          :    2.00 (sec)

# Data Process Condition
    Smoothing                  [ AUTO ]
          smoothing points     : 11
    B.G.Subtruction            [ AUTO ]
          sampling points      : 13
          repeat times         : 30
    Ka1-a2 Separate            [ MANUAL ]
          Ka1 a2 ratio         : 50 (%)
    Peak Search                [ AUTO ]
          differential points  : 11
          FWHM threhold        : 0.050 (deg)
          intensity threhold   : 30 (par mil)
          FWHM ratio  (n-1)/n  : 2
    System error Correction    [ NO ]
    Precise peak Correction    [ NO ]
```

< Group: LeeZhiHua Data: CaOmnOLow >